

---

## Evidence for methane isotopic bond re-ordering in gas reservoirs sourcing cold seeps from the Sea of Marmara

Giunta Thomas <sup>1,2,\*</sup>, Labidi J. <sup>3,4</sup>, Kohl I.E. <sup>4</sup>, Ruffine Livio <sup>1</sup>, Donval Jean-Pierre <sup>1</sup>, Géli Louis <sup>1</sup>, Çaçatay M.N. <sup>5</sup>, Lu H. <sup>6</sup>, Young E.D. <sup>4</sup>

<sup>1</sup> IFREMER, Unité des Géosciences Marines, 29280 Plouzané, France

<sup>2</sup> Université de Bretagne Occidentale, Laboratoire Géosciences Océan, 29280 Plouzané, France

<sup>3</sup> Université de Paris, Institut de Physique du Globe de Paris, CNRS, F-75005 Paris, France

<sup>4</sup> University of California Los Angeles, Department of Earth, Planetary and Space Sciences, CA 90095, Los Angeles, USA

<sup>5</sup> Istanbul Teknik University, Faculty of Mines, Department of Geological Engineering, TR-34469 Istanbul, Turkey

<sup>6</sup> Peking University, Department of Energy & Sciences, College of Engineering, Beijing 100871, China

\* Corresponding author : Thomas Giunta, email address : [thomas.giunta@ifremer.fr](mailto:thomas.giunta@ifremer.fr)

---

### Abstract :

The measurement of methane clumped isotopologues ( and ) allows exploring isotope bond ordering within methane molecules, and may reveal equilibrium temperatures. Whether such temperature reflects the formation or re-equilibration temperature of the methane is not well understood, but would have critical implications for the use of methane clumped isotopologues as geo-thermometers. Here we investigate gas bubbles from vigorous emissions at cold seeps (n = 14) in the Sea of Marmara, Turkey. These cold seeps are sourced from deeper sedimentary reservoirs. Conventional geochemical tracers such as carbon and hydrogen bulk isotopic ratios ( $^{13}\text{C}/^{12}\text{C}$  and D/H) or n-alkane molecular ratios, suggest these gases reflect various degrees of mixing between thermogenic and microbial sources. Some samples would generally be considered purely microbial in origin (; ‰). We report measurements of and showing that a fraction of those gases are in internal thermodynamic equilibrium, with the abundances of the two mass-18 isotopologues indicating concordant temperatures of  $\sim 90$  °C and  $\sim 130$  °C. These concordant temperatures are recorded by gases of putative microbial and thermogenic origin; the temperatures of equilibration are irrespective of the formation mechanism of the gases. We conclude that the two high-temperatures recorded by and are best explained by non-enzymatic re-equilibration at two local subsurface temperatures. First principles suggest that unequal rates of exchange are possible. Disequilibrium signatures where the two isotopologues yield discordant apparent temperatures are exhibited by other samples. In those cases the data define a trend of variable at nearly constant . These signatures are enigmatic, and we investigate and reject multiple possible explanations including mixing, diffusion or Anaerobic Oxidation of Methane. Different rates of re-equilibration between the two rare isotopologues are implied, although lacks experimental foundation at present. In general, all of these data point towards re-equilibration of the mass-18 methane isotopologues as an important process.

---

## Highlights

►  $\Delta^{13}\text{CH}_3\text{D}$  and  $\Delta^{12}\text{CH}_2\text{D}_2$  investigated in marine cold seeps from the Sea of Marmara. ► Microbial/thermogenic samples show equilibrium temperatures up to 130 °C. ► Non-enzymatic mechanism for isotope bond ordering to reservoirs temperatures.

**Keywords** : cold seeps, methane, clumped isotopologues, bond-ordering

## 42 1. Introduction

43 In most natural settings, the generation of hydrocarbon gases results from the degradation in the  
44 subsurface of organic-rich sedimentary horizons, either through thermocatalytic cracking (i.e. referred  
45 as thermogenic generation), or through microbial reduction of oxidized carbon-bearing species (i.e.  
46 microbial methanogenesis). Geochemical investigations of methane and other light hydrocarbons have  
47 historically been undertaken using bulk stable isotope ratios of carbon and hydrogen ( $\delta^{13}\text{C}$  and  $\delta\text{D}$ ), as  
48 well as molecular ratios of light *n*-alkanes (e.g. Bernard et al., 1976; Schoell, 1988). For example,  
49 thermogenic gases are expected to contain methane and variable (but significant) amount of  $\text{C}_{2+}$  gases  
50 (i.e. non-methane *n*-alkanes), with  $\delta^{13}\text{C}$  and  $\delta\text{D}$  values evolving as a function of the thermal maturity  
51 (Schoell, 1988; Tang et al., 2000) whereas microbial gases are overwhelmingly composed of methane  
52 (Martini et al., 1998) with  $\delta^{13}\text{C}$  and  $\delta\text{D}$  being generally lower than methane of thermogenic origin.

53 Recent advances in high-resolution mass-spectrometry and in laser absorption spectroscopy  
54 have allowed the measurement of the relative abundances of doubly-substituted methane isotopologues  
55 (i.e. methane molecules containing two heavy isotope substitutions)  $^{13}\text{CH}_3\text{D}$  (Stolper et al., 2014a; Ono

56 et al., 2014; Young et al., 2016) and  $^{12}\text{CH}_2\text{D}_2$  (Young et al., 2016; Eldridge et al., 2019; Gonzalez et al.,  
57 2019). These abundances are usually reported as per mil deviations from the “stochastic” isotopologue  
58 abundances that would occur with random distributions of isotopes across all species,  $\Delta^{13}\text{CH}_3\text{D}$  and  
59  $\Delta^{12}\text{CH}_2\text{D}_2$ . This novel approach allows the investigation of isotope bond ordering in methane  
60 molecules. At thermodynamic equilibrium  $\Delta^{13}\text{CH}_3\text{D}$  and  $\Delta^{12}\text{CH}_2\text{D}_2$  provide independent measurements  
61 of temperature of formation or equilibration. Where the two temperatures do not agree, kinetic  
62 processes or mixing is implied.

63 Rare mass-18 methane isotopologues have been shown to provide apparently reliable formation  
64 temperatures in numerous natural settings, from thermogenic (Stolper et al., 2014b; 2015; Wang et al.,  
65 2015, Douglas et al., 2016; Young et al., 2017; Giunta et al., 2019), to hydrothermal (Wang et al., 2015,  
66 2018) and even possibly to some microbially-dominated settings (Stolper et al., 2015; Wang et al.,  
67 2015; Inagaki et al., 2015). Yet, the idea that methane ‘clumped’ isotopes would reflect the formation  
68 temperature requires that methane is synthesized at thermodynamic equilibrium. This later requirement  
69 is puzzling because methane generation, whether thermogenic, microbial or abiotic, is always  
70 considered to be controlled by kinetic effects rather than by thermodynamic equilibrium (e.g. Berner  
71 and Faber, 1996; McCollom, 2013). In the laboratory, the role of kinetic isotope effects on clumped  
72 isotopes is clear, especially for microbial generation, and laboratory experiments generally yield  
73 disequilibrium signatures (Stolper et al., 2015; Wang et al., 2015; Douglas et al., 2016; Young et al., 2017;  
74 Shuai et al., 2018; Gruen et al., 2018; Giunta et al., 2019), belying temperature information. Note that  
75 these disequilibrium signatures associated with microbial or low-temperature abiotic methane are also  
76 observable in nature, especially when measurements of both  $\Delta^{13}\text{CH}_3\text{D}$  and  $\Delta^{12}\text{CH}_2\text{D}_2$  are combined  
77 (Young et al., 2017; Giunta et al., 2019). In contrast, thermogenic methane in sedimentary basins seems  
78 to show evidence for equilibrium relative abundances of  $\text{CH}_4$  isotopologues (Young et al., 2017,

79 [Giunta et al., 2019](#)) and it is unclear whether this could reflect a formation temperature or a re-  
80 equilibration that occurred after formation.

81 In this study, we investigate methane emitted from vigorous free-gas vents at cold seep sites in  
82 the Sea of Marmara (SoM, see Fig. 1) ([Geli, et al., 2008](#); [Bourry et al., 2009](#); [Ruffine et al., 2018a](#)).  
83 These vents are sourced by underlying sedimentary reservoirs ([Ruffine et al., 2018b](#); [Géli et al., 2018](#)).  
84 Combining gas composition with carbon and hydrogen stable isotope analyses, two main origins of gas  
85 were identified ([Ruffine et al., 2018b](#)). Gases sampled on the structural highs, the Western High and  
86 Central High, are thought to be thermogenic in origin, whereas gases sampled in the southern flank of  
87 the Tekirdağ Basin and in the Çınarcık Basin are thought to be essentially microbial in origin. Other  
88 gases from the area were interpreted to reflect various proportions of mixing between these two types  
89 of sources. Hydrate formation or destabilization is unlikely to have affected these gases. All gases were  
90 collected at locations where thermodynamic conditions for hydrate stabilization are not met with the  
91 exception of samples collected in the Western High ([Ruffine et al., 2012](#); [2018b](#)). In contrast, the  
92 chemical and isotopic compositions have been all accounted for by mixing. Mixing as illustrated in Fig.  
93 2 using the methane  $\delta^{13}\text{C}$  versus  $\text{C}_1/\text{C}_{2+}$  ratios ([Ruffine et al., 2018b](#)). Thermogenic gases are typically  
94 thought to contain significant amounts of  $\text{C}_{2+}$  gases and therefore to show low  $\text{C}_1/\text{C}_{2+}$  ratios together  
95 with relatively enriched methane  $\delta^{13}\text{C}$  values (e.g. [Bernard et al., 1976](#)). In contrast, microbial gases are  
96 expected to be dominated by methane with trace amounts of  $\text{C}_{2+}$  gases and are therefore expected to  
97 have high  $\text{C}_1/\text{C}_{2+}$  ratios together with relatively low  $\delta^{13}\text{C}$  values. Thus, mixing between thermogenic  
98 and a microbial end members is predicted to produce a characteristic mixing hyperbola (Fig. 2). Some  
99 samples from the SoM however – especially gases from the Central High and from the western flank of  
100 the Tekirdağ Basin – appear to deviate from this mixing line. These gases were noted to show  
101 anomalously heavy propane  $\delta^{13}\text{C}$  ([Ruffine et al., 2018b](#)), comprising evidence for biodegradation of  
102 propane ([James and Burns, 1984](#)) which could explain the departure from the two endmembers mixing

103 line (Fig. 2). In this study, we explore further these hypotheses by combining the measurement of  
104  $^{13}\text{CH}_3\text{D}$  and  $^{12}\text{CH}_2\text{D}_2$  to provide additional constraints on the thermal history of methane in the  
105 sedimentary reservoirs feeding the Marmara cold vents.

106

## 107 **2. Geological setting and fluid activity**

108 The Sea of Marmara (SoM) is an interior sea located in the Turkish territory and links the Black  
109 sea to the northeast and the Mediterranean sea to the west via the Bosphorus and the Dardanelle straits,  
110 respectively. The SoM is composed of three basins, the Tekirdağ Basin, the Central Basin and the  
111 Çınarcık Basin, which latter reaches a maximum depth of 1273 m. Each of the basins are separated by  
112 push-up structures, the Western High and the Central High (see Fig. 1). The SoM seafloor is cut  
113 lengthwise by a dense network of faults belonging to the North Anatolian Fault (NAF) system which  
114 accommodates the slip motion between the Eurasian plate and the Anatolian block (e.g. [Armijo et al.,](#)  
115 [1999](#)). In the northern part of this network, the Main Marmara Fault is seismically the most active  
116 sequence of fault segments in the region, having caused devastating earthquakes in the past (e.g.  
117 [Ambraseys and Jackson, 2000](#)).

118 At the seafloor, cold seeps with fluid and gas emissions are widespread across the SoM, but  
119 appear to be more frequent near active faults (e.g. [Geli et al., 2008](#)), perhaps suggesting a relationship  
120 between pressurized gas reservoirs and seismic activity ([Gasperini et al., 2011](#); [Geli et al., 2018](#)). The  
121 sampling of free-gas (i.e. bubbles) emanating at the SoM seafloor was first achieved during the Marsite  
122 cruise in 2007, after detection of gas seep locations using a SIMRAD-EK60 echo sounder and acoustic  
123 anomalies associated to gas bubbles in the water column ([Geli et al., 2008](#)). At the time, only three  
124 active gas sites were sampled in the Çınarcık Basin, in the Western High and in the Central High  
125 ([Bourry et al., 2009](#)). In 2014, a more extensive study on gases discharged at the SoM seafloor along  
126 the NAF was undertaken during the Marsite Cruise ([Ruffine et al., 2018a,b](#)). Through combination of

127 acoustic survey and ROV dives, new active sites were discovered and sampled in the Çınarcık Basin, in  
128 the Western High and in the Central High, as well as in the Tekirdağ Basin (Ruffine et al., 2018b).  
129 Gases that are venting at the seafloor consist mainly of methane-rich mixtures (up to > 99 %-mol),  
130 some of which containing significant amount of other hydrocarbon. The contribution of light *n*-alkanes  
131 is thought to reflect hydrocarbon formation within sediments in the SoM via organic matter  
132 degradation, both thermocatalytic cracking of organic matter and microbial reduction of oxidized  
133 carbon-bearing species have been suggested (Gürgey et al., 2005; Ruffine et al., 2018b).

134

### 135 3. Methods

136 Gas samples were collected in the course of the Marsite Cruise in November 2014. Method for  
137 gas sampling and preservation are outlined in details in Ruffine et al., (2015, 2018b). Seafloor gas vents  
138 were identified by coupling water column acoustic guiding and visual inspection with the ROV Victor  
139 6000. The most vigorous gas vents were then sampled with the PEGAZ sampler, a sampling device  
140 manipulated by the ROV which is designed to sample gas bubbles and preserve them at *in situ*  
141 pressure. Gas aliquots were then sub-sampled at pressure ranging between 2 and 4 bars in 12 mL Labco  
142 vials. These Labco vials were then used for measuring the gas composition (light alkanes, N<sub>2</sub> and CO<sub>2</sub>  
143 contents) as well as bulk isotope geochemistry ( $\delta^{13}\text{C}$ ,  $\delta\text{D}$ ) on light alkane (including methane). All these  
144 isotope analyses were performed at ISOLAB in the Netherlands. Results were reported and discussed  
145 by Ruffine et al., (2018b).

146 Methane gas samples were purified and analyzed at UCLA to obtain methane isotopologue  
147 abundances. The ratios  $^{13}\text{CH}_3\text{D}/^{12}\text{CH}_4$ ,  $^{12}\text{CH}_2\text{D}_2/^{12}\text{CH}_4$ ,  $^{13}\text{CH}_4/^{12}\text{CH}_4$ , and  $^{12}\text{CH}_3\text{D}/^{12}\text{CH}_4$  are measured  
148 with the prototype Nu Instruments Panorama, a high-resolution gas-source double-focusing mass  
149 spectrometer at UCLA. Mass-18 isotopologue compositions are reported versus a stochastic

150 distribution (Wang et al., 2004), representing a theoretically infinite temperature, and expressed in per  
151 mil using the capital delta notation:

152

$$153 \Delta^{13}\text{CH}_3\text{D} = [({}^{13}\text{CH}_3\text{D}/{}^{12}\text{CH}_4)_{\text{sample}}/({}^{13}\text{CH}_3\text{D}/{}^{12}\text{CH}_4)_{\text{stochastic}} - 1] \times 1000 \quad (1)$$

154

155 and

156

$$157 \Delta^{12}\text{CH}_2\text{D}_2 = [({}^{12}\text{CH}_2\text{D}_2/{}^{12}\text{CH}_4)_{\text{sample}}/({}^{12}\text{CH}_2\text{D}_2/{}^{12}\text{CH}_4)_{\text{stochastic}} - 1] \times 1000 \quad (2).$$

158

159 Methods for sample purification and isotope ratio measurements are outlined in detail by Young et al.,  
160 (2016, 2017) and briefly summarized here. Prior to measurements of isotopologues, methane is purified  
161 on a vacuum line interfaced with a gas chromatograph (GC). Two GC columns are coupled in series  
162 using He as the carrier gas. The first column consists of a 3-m long, 1/8-inch OD stainless steel tubing,  
163 packed with 5A molecular sieve and is used to separate H<sub>2</sub>, Ar, O<sub>2</sub> and N<sub>2</sub> from CH<sub>4</sub> and other alkanes.  
164 The second column is used to separate CH<sub>4</sub> from other hydrocarbons and consists of a 2-m long 1/8-  
165 inch OD stainless steel tubing packed with HayeSep D porous polymer. Peaks are identified on a  
166 passive TCD. In order to measure <sup>12</sup>CH<sub>4</sub><sup>+</sup>, <sup>13</sup>CH<sub>4</sub><sup>+</sup>, <sup>12</sup>CH<sub>3</sub>D<sup>+</sup>, <sup>13</sup>CH<sub>3</sub>D<sup>+</sup> and <sup>12</sup>CH<sub>2</sub>D<sub>2</sub><sup>+</sup> ion currents, the mass  
167 spectrometer is set to a mass resolving power equal to or greater than 40000. This allows resolving of  
168 the two mass-18 isotopologues (<sup>13</sup>CH<sub>3</sub>D and <sup>12</sup>CH<sub>2</sub>D<sub>2</sub>), both measured on the axial collector with an  
169 electron multiplier. Meanwhile, mass-16 and mass-17 isotopologues are measured on Faraday  
170 collectors with amplifier resistors of 10<sup>11</sup> Ω. Sample and reference bellows are adjusted so that ion  
171 current intensities are balanced. The current intensities are rebalanced after each measurement cycle. At  
172 first, the magnet is set to measure simultaneously <sup>12</sup>CH<sub>3</sub>D<sup>+</sup>/<sup>12</sup>CH<sub>4</sub><sup>+</sup> and <sup>12</sup>CH<sub>2</sub>D<sub>2</sub><sup>+</sup>/<sup>12</sup>CH<sub>4</sub><sup>+</sup> ratios, with  
173 <sup>12</sup>CH<sub>2</sub>D<sub>2</sub><sup>+</sup> (18.04385 amu) being measured on the axial collector. In a second setting, the magnet is set to



174 measure  $^{13}\text{CH}_3\text{D}^+$  (18.04090 amu) on the axial collector, and  $^{13}\text{CH}_4^+ / ^{12}\text{CH}_4^+$  and  $^{13}\text{CH}_3\text{D} / ^{12}\text{CH}_4^+$  ratios are  
175 measured simultaneously. Overall, the external  $1\sigma$  error ( $n=5$ ) including both the accuracy and the  
176 reproducibility is estimated to be  $\pm 0.1$  ‰ for  $\Delta^{13}\text{CH}_3\text{D}$ ,  $\pm 0.8$  ‰ for  $\Delta^{12}\text{CH}_2\text{D}_2$ ,  $\pm 0.1$  ‰ for  $\delta^{13}\text{C}$ , and  
177 of approximately  $\pm 0.3$  ‰ for  $\delta\text{D}$ . Note that the measurements of methane  $\delta^{13}\text{C}$  and  $\delta\text{D}$  values  
178 performed conjointly with the rare methane isotopologues are within uncertainties of measurements  
179 previously performed at ISOLAB.

180

#### 181 4. Results

182 The measurements of  $\Delta^{13}\text{CH}_3\text{D}$  and  $\Delta^{12}\text{CH}_2\text{D}_2$  allow the description of methane isotopic bond-  
183 ordering in a given sample. At thermodynamic equilibrium both  $\Delta^{13}\text{CH}_3\text{D}$  and  $\Delta^{12}\text{CH}_2\text{D}_2$  should be  
184 concordant in recording the same temperature of equilibrium. The data are shown in Figure 3, together  
185 with the theoretical thermodynamic equilibrium curve (Young et al., 2016). Samples DV04-PE02,  
186 DV04-PE08, DV01-PE02, DV03-PE03 and DV05-PE02 appear close to equilibrium, though they show  
187 two populations of  $\Delta^{13}\text{CH}_3\text{D}$  and  $\Delta^{12}\text{CH}_2\text{D}_2$  values (Fig. 3b). The first group composed of samples  
188 DV03-PE03 and DV05-PE02 define average  $\Delta^{13}\text{CH}_3\text{D}$  and  $\Delta^{12}\text{CH}_2\text{D}_2$  values of  $3.45 \pm 0.1$  ‰ and  
189  $8.88 \pm 0.4$  ‰ yielding apparent concordant temperatures of  $127_{-5}^{+5}$  °C and  $135_{-7}^{+7}$  °C, respectively.  
190 These consistent temperatures are indistinguishable, and suggest that isotope ordering was in response  
191 to thermodynamic equilibrium in these samples. The second group composed of samples DV01-PE02,  
192 DV04-PE02 and DV04-PE08, define average  $\Delta^{13}\text{CH}_3\text{D}$  and  $\Delta^{12}\text{CH}_2\text{D}_2$  of  $4.40 \pm 0.16$  ‰ and  
193  $11.96 \pm 0.32$  ‰, yielding nearly concordant apparent temperatures of  $77_{-8}^{+7}$  °C and  $92_{-4}^{+4}$  °C, respectively.  
194 The remaining samples appear shifted to the right of the equilibrium curve to varying degrees, i.e. they  
195 show higher  $\Delta^{13}\text{CH}_3\text{D}$  values at a given  $\Delta^{12}\text{CH}_2\text{D}_2$  relative to equilibrium (Fig. 3b). For these, it is not  
196 clear whether any temperature information can be *a priori* obtained from either  $\delta^{13}\text{C}$  or  $\delta\text{D}$ .  
197 Probability density plots indicate that the distribution of  $\Delta^{12}\text{CH}_2\text{D}_2$  values is bi-modal (Fig. 3b), with

198 peaks at  $8.01 \pm 1.08$  ‰ and  $11.88 \pm 0.44$  ‰, corresponding to apparent temperatures of  $152 \pm 22$  °C and  
199  $93 \pm 5$  °C, respectively. These two temperatures are remarkably similar to maximum temperatures  
200 reached by two main source rocks in the area, the Eocene Hamitabad Formation and the Oligocene  
201 Mezardere Formation (Huvaz et al., 2005; Gürgey, 2009).

202 Samples from the western flank of the Tekirdağ Basin (DV03) may be taken as a telling  
203 illustration of the overall complexity of our dataset. These gases show the widest variability in methane  
204 doubly-substituted isotopologue signatures, with  $\Delta^{13}\text{CH}_3\text{D}$  ranging from 3.4 to 6.3 ‰, and  $\Delta^{12}\text{CH}_2\text{D}_2$   
205 ranging from 5.7 to 11.2 ‰. These samples also show the largest variability in  $C_1/C_{2+}$  values ranging  
206 from 10 to 1560 (Fig. 2), and bulk  $\delta^{13}\text{C}$  ranging from -41.2 to -58 ‰ (Fig. 2, Fig.3a). However,  
207 perhaps most curious is that two samples, DV03-PE01 and DV03-PE06 are nearly identical both in  
208 their gas composition and in their bulk isotopic signatures (Fig. 2, Fig. 3a), and yet show significantly  
209 different  $\Delta^{13}\text{CH}_3\text{D}$  values at a given  $\Delta^{12}\text{CH}_2\text{D}_2$ , being members of the two distinct groups defined by the  
210 two peaks in  $\Delta^{12}\text{CH}_2\text{D}_2$  values (Fig. 3b). This is also true for samples from the Çınarcık Basin (DV05)  
211 and, though less significant, for samples from the southeastern flank of the Tekirdağ Basin (DV04. All  
212 of these samples have been previously interpreted as dominantly microbial in origin (Ruffine et al.,  
213 2018). In other words, we observe a decoupling between conventional tracers and clumped methane  
214 signatures.

215 Decoupling also appears for some samples which are distinct in gas composition and in bulk  
216 isotope signatures but are similar in the isotopologue space (Fig. 3b). The most striking case are the  
217 DV03-PE03 (Tekirdağ Basin) and the DV05-PE02 (Çınarcık Basin) samples. They both plot on (or  
218 near) the equilibrium curve at an equivalent temperature of  $\sim 130$ °C. However, they have distinct bulk  
219 isotope compositions. Sample DV03-PE03 shows relatively high  $\delta^{13}\text{C}$  (of -41.2 ‰) together with low  
220  $C_1/C_{2+}$  (of 10) which could reflect a thermogenic end-member (Ruffine et al., (2018b) similar to oil-  
221 associated gases found in the Thrace Basin (Huvaz et al., 2005; Gürgey, 2009). An apparent

222 equilibrium temperature of  $\sim 130^{\circ}\text{C}$  derived from both  $\Delta^{13}\text{CH}_3\text{D}$  and  $\Delta^{12}\text{CH}_2\text{D}_2$  would indicate a  
223 temperature generally consistent with the typical range expected for thermogenic gas generation (Tissot  
224 and Welte, 1978). On the other hand, based on the lack of  $\text{C}_{2+}$  ( $\text{C}_1/\text{C}_{2+} = 1456$ ) and low  $\delta^{13}\text{C}$  and  $\delta\text{D}$   
225 values  $-63\text{‰}$  and  $-251\text{‰}$  respectively, sample DV05-PE02 appears microbial in origin (i.e. derived  
226 from microbial methanogenesis). For this sample, apparent temperatures of  $124_{-6}^{+6}\text{°C}$  and  $139_{-13}^{+14}\text{°C}$ ,  
227 derived from  $\Delta^{13}\text{CH}_3\text{D}$  and  $\Delta^{12}\text{CH}_2\text{D}_2$  respectively, are within uncertainty of the upper temperature limit  
228 for life of  $\sim 121\text{°C}$  (Kashefi and Lovley, 2003; Takai et al., 2008).

229 Overall, variations observed in the  $\Delta^{13}\text{CH}_3\text{D}$  and  $\Delta^{12}\text{CH}_2\text{D}_2$  space do not correlate with bulk  
230 isotope ratios or in  $\text{C}_1/\text{C}_{2+}$ . This suggests that the isotope bond ordering is responding to forcings that  
231 are not obviously related to gas composition or bulk isotope ratios.

232

## 233 5. Discussion

### 234 5.1. Isotope-bond reordering

235 First studies on methane isotopologues have provided consistent observations when  
236 investigating methane of thermogenic or microbial origin. Apparent agreement between  $\Delta^{13}\text{CH}_3\text{D}$ -  
237 based temperatures and measured environmental temperatures, or expected formation temperatures  
238 were observed for most thermogenic gases (Stolper et al., 2014b, 2015, 2017; Wang et al., 2015;  
239 Douglas et al., 2016). In addition, concordant temperature from both  $\Delta^{12}\text{CH}_2\text{D}_2$  and  $\Delta^{13}\text{CH}_3\text{D}$  in the  
240 same samples supports the idea that thermogenic methane in natural settings is generally at ‘bond  
241 ordering’ equilibrium (Young et al., 2017; Giunta et al., 2019). Yet, the mechanism by which  
242 isotopologues reach equilibrium in nature is still unclear, as thermogenic generation is generally  
243 thought to be controlled by kinetics (e.g. Clayton, 1991; Tang et al., 2000; Stolper et al., 2017; Xia and  
244 Gao, 2019). Recently, experimental and modeling works have also shown that disequilibrium

245 signatures could be expected during gas generation and/or accumulation in reservoirs (Shuai et al.,  
246 2018; Xia and Gao, 2019), yet it does not seem to be common in most natural settings.

247 On the other hand, microbial methane is associated with large isotopologue disequilibrium  
248 under laboratory conditions, often yielding negative  $\Delta^{13}\text{CH}_3\text{D}$  (Wang et al., 2015; Stolper et al., 2015;  
249 Young et al., 2017; Douglas et al., 2017 Gruen et al., 2018; Giunta et al., 2019) and markedly negative  
250  $\Delta^{12}\text{CH}_2\text{D}_2$  values (Young et al., 2017; Giunta et al., 2019; Gonzalez et al., 2019) (Fig. 4). The causes of  
251 the disequilibrium are beyond the scope of this study but may include: the rate of methanogenesis (e.g.  
252 Wang et al., 2015, Stolper et al., 2015), the metabolic pathways (Giunta et al., 2019; Young 2019),  
253 statistical combinatorial effects (Young et al., 2017; Cao et al., 2019; Taenzer et al., 2020), and/or  
254 quantum tunneling effects (Young et al., 2017; 2019). In natural settings, disequilibrium signatures  
255 similar to those observed in laboratory are commonly observed (e.g. Wang et al., 2015; Douglas et al.,  
256 2016; Giunta et al., 2019; Young, 2019), however, there are certain environments, such as in marine  
257 sediments, where isotopologue signatures appear closer to equilibrium with environmental  
258 temperatures (e.g. Wang et al., 2015; Stolper et al., 2015; Douglas et al., 2016; Inagaki et al., 2015;  
259 Giunta et al., 2019; Ash et al., 2019). This led some authors to propose that isotopologue signatures  
260 during microbial methanogenesis would be largely controlled by the degree of metabolic reversibility  
261 (Wang et al., 2015; Stolper et al., 2015), and may sometimes, especially in the deep biosphere, result in  
262 methane in isotopologue equilibrium. Young et al. (2017) argued that microbial communities may drive  
263 methane towards equilibrium in nature, and Young (2019) presented preliminary evidence for the  
264 potential role of methanotrophic organisms performing Anaerobic Oxidation of Methane (AOM) in re-  
265 ordering atomic bonds within methane molecules towards the equilibrium (also supported by Giunta et  
266 al., 2019). Ash et al. (2019) presented evidence that AOM causes methane to achieve equilibrium  
267  $\Delta^{13}\text{CH}_3\text{D}$  and  $\Delta^{12}\text{CH}_2\text{D}_2$  values in the sediments from the Bornholm Basin, Baltic Sea. Both proposed  
268 mechanisms for equilibration lack unequivocal experimental validation at present.

269 In SoM gases, samples DV03-PE03 and DV01-PE02 were identified as dominantly  
270 thermogenic in origin (Ruffine et al., 2018b) and define two distinct but concordant temperatures of  
271  $\sim 130$  °C and  $\sim 90$  °C, respectively (Fig. 3b). Both temperatures are consistent with the ‘gas window’ for  
272 thermogenic generation (Tissot and Welte, 1978) and with maximum temperatures reached by two  
273 main source rocks in the area, the Eocene Hamitabad Formation and the Oligocene Mezardere  
274 Formation (Huvaz et al., 2005; Gürgey, 2009). We therefore interpret these data as recording  
275 characteristic regional temperatures for methane equilibration.

276 In contrast, samples DV05-PE02, DV04-PE02 and DV04-PE08 are considered to be dominantly  
277 microbial in origin on the basis of  $\delta^{13}\text{C} < -60$  ‰ and  $\text{C}_1/\text{C}_{2+} > 1000$ , but nonetheless plot on (or near)  
278 the equilibrium curve at temperatures of  $\sim 90$  and  $\sim 130$  °C, the same two temperatures recorded by the  
279 thermogenic samples (Fig. 3b). It is unlikely that these relatively high temperatures for nominally  
280 microbial gases are the result of hyper-thermophilic activity in sediments of the SoM. A temperature of  
281  $\sim 130$  °C slightly exceeds the upper temperature limit for life of  $\sim 121$  °C, a maximum that has so far  
282 only been observed for optimal laboratory conditions and for archeal strains that are typical of energy-  
283 rich hydrothermal vent environments (Kashefi and Lovley, 2003; Takai et al., 2008). The temperature  
284 limit for microbial degradation of organic matter in subsurface sedimentary settings that are nutrient-  
285 starved systems [REF] is considered to be 80-90°C (Head et al., 2003), and possibly even lower at  
286  $\sim 60$  °C in deeply buried sediments (Inagaki et al., 2015). For these reasons, we conclude that an  
287 equilibrium temperature of  $\sim 130$  °C for natural methane with microbial traits must necessary reflect a  
288 ‘non-enzymatic’ (i.e. abiotic) re-equilibration to a temperature reached during sediment burial, rather  
289 than the actual temperature of formation of microbial methane in the subsurface. This explanation may  
290 also hold true for putative microbial methane equilibrated at temperatures of  $\sim 90$  °C (DV04-PE04 and  
291 DV04-PE08). The implication is that the production and accumulation of microbial methane occurred  
292 prior to burial, after which it re-equilibrated upon the heating that attended burial. Accordingly, we this

293 can not exclude that thermogenic gases now appearing on the equilibrium  $\Delta^{12}\text{CH}_2\text{D}_2$  vs.  $\Delta^{13}\text{CH}_3\text{D}$  curve  
294 have inherited their equilibrium signature from a similar re-equilibration mechanism, rather than from  
295 their actual formation.

296 Rates for re-equilibration of  $^{13}\text{CH}_3\text{D}/^{12}\text{CH}_4$  and  $^{12}\text{CH}_2\text{D}_2/^{12}\text{CH}_4$  isotopologue ratios, especially at  
297 relatively low temperatures, are unknown. Wang et al., (2018) have speculated that rates for re-  
298 equilibration of  $^{13}\text{CH}_3\text{D}$  may follow the rates for ‘external’, or inter-species re-equilibration of D/H  
299 ratios between methane and water in hydrothermal systems. They extrapolated from a small body of  
300 experimental data at 200, 323 and 400 °C that the timescale for  $\text{CH}_4$  isotopic bond re-ordering in the  
301 absence of a metal catalyst would be on the order of  $10^9$  years for temperature of 150 °C, and  $> 10^{10}$   
302 years below 100 °C. This would suggest that the relative abundances of methane isotopologues are not  
303 subject to resetting in most sedimentary settings. This conclusion appears to be contradicted by our  
304 observations. In fact, our dataset argues in favor of faster isotopologue re-ordering rates than those for  
305 inter-species isotope exchange with environmental (reservoir) waters. Our data requires that methane  
306 re-equilibration at rather cool ( $< 150$  °C) subsurface conditions can occur, promoted or catalyzed by a  
307 mechanism that remains to be identified. Recently, a similar process was suggested to account for  
308  $^{12}\text{CH}_2\text{D}_2$  re-ordering down to 65 °C with no resolvable  $^{13}\text{CH}_3\text{D}$  re-equilibration in well characterized  
309 marine hydrothermal vent fluids (Labidi et al., 2020).

310 From this data-set, it is clear that we cannot determine with certainty whether methane achieved  
311 bond equilibrium via exchange with other molecules. Source reservoirs are not readily accessible to  
312 sampling, precluding assessments of inter-species (e.g.,  $\text{CH}_4$  and  $\text{H}_2\text{O}$ ) isotopic exchange. The fact that  
313 samples DV05-PE02 and DV05-PE03 have identical  $\delta\text{D}$  values, but distinct  $\Delta^{13}\text{CH}_3\text{D}$  values, one at  
314 equilibrium based on concordance with  $\Delta^{12}\text{CH}_2\text{D}_2$ , and the other not, may indicate that re-equilibration  
315 among methane molecules can occur without significant isotope exchange with other molecular species  
316 that would cause shifts in the methane bulk  $\delta\text{D}$  values. The alternative is that these two samples have

317 reached D/H equilibrium with the same source of hydrogen but did not reach mass-18 isotopologue  
318 equilibrium. In either case, it appears as though rates for bond re-equilibration and for inter-species re-  
319 equilibration are decoupled.

320 The probability distributions in Fig. 3b suggest that  $\Delta^{12}\text{CH}_2\text{D}_2$  has experienced a greater degree  
321 of re-equilibration than  $\Delta^{13}\text{CH}_3\text{D}$ . We investigate the prospects for this in greater detail in Section  
322 5.2.4. The catalysis of hydrogen isotope exchange among alkanes has been studied for almost a century  
323 (see recent review by [Sattler, 2018](#)), but remains poorly understood for temperatures and timescales  
324 that might be relevant for geological applications. Transition metals are well known to catalyze  
325 hydrogen exchange with methane ([Horibe and Craig, 1995](#)) and have been shown to promote  
326 isotopologue equilibrium at temperatures above 150 °C ([Stolper et al., 2014](#); [Ono et al., 2014](#); [Young et  
327 al., 2016](#)). Recent studies have also demonstrated the potential of aluminum oxide (in the form of  $\gamma$ -  
328 alumina) in promoting re-equilibration of methane to temperatures as low as 1 °C ([Wang et al., 2019](#);  
329 [Eldridge et al., 2019](#)). In both cases, it is not clear how this type of catalysis can be relevant to  
330 sedimentary environments. Alternatively, exchange mediated by clay mineral surfaces might be a  
331 process to consider, as clays are known to promote hydrogen exchange on larger organic molecules  
332 ([Alexander et al., 1982](#), [Sessions et al., 2004](#)).

333

## 334 5.2. Departures from Equilibrium

### 335 5.2.1. *Mixing*

336 Methane samples that do not record concordant temperatures of ~90 and ~130 °C exhibit  
337 variable but significant degrees of disequilibrium, all plotting to the right of the equilibrium curve in  
338 Fig. 3b and exhibiting relatively large variations in  $\Delta^{13}\text{CH}_3\text{D}$  and relatively small variations in  
339  $\Delta^{12}\text{CH}_2\text{D}_2$ . Based on bulk isotope ratios and molecular ratios, these gases may have  $\Delta^{12}\text{CH}_2\text{D}_2$  and  
340  $\Delta^{13}\text{CH}_3\text{D}$  values resulting from mixing between thermogenic and microbial gases (Fig. 2; [Ruffine et al.,](#)

341 [2018b](#)). However, mixing, if it occurred, may now be disguised by varying degrees of re-equilibration  
342 based on the evidence summarized in Fig. 3b. Nonetheless, vestiges of disequilibrium in isotopologue  
343 space due to mixing may persist. In general, the samples showing the largest offset from the  
344 equilibrium curve (DV03-PE01, DV03-PE09 and DV05-PE03) are considered to be dominantly  
345 microbial in origin based on bulk isotope ratios and the molecular concentrations comprising the gas.  
346 This suggests that one end-member for mixing was microbial, perhaps having  $\Delta^{12}\text{CH}_2\text{D}_2$  and  $\Delta^{13}\text{CH}_3\text{D}$   
347 values characteristic of microbial methanogenesis in the laboratory and in some natural settings. The  
348 magnitude of the disequilibrium observed in our data is much less than that obtained from microbial  
349 methanogenesis in laboratory cultures ([Young et al., 2017](#)) and from samples of microbial  
350 methanogenesis origin in natural settings investigated to date where both  $\Delta^{13}\text{CH}_3\text{D}$  with  $\Delta^{12}\text{CH}_2\text{D}_2$  have  
351 been measured ([Giunta et al., 2019](#); [Young 2019](#)) (Fig. 4). Invoking a microbial end-member with a  
352 signature similar to those measured in the laboratory would imply that the most disequilibrated samples  
353 in this study are composed of no more than 40 to 60 % microbial methane (Fig. 4). While mixing of  
354 this end-member with a thermogenic component explains the isotopologue data (Fig. 4), this relatively  
355 low fraction of microbial methane would be inconsistent with their  $C_1/C_{2+} > 1000$  usually considered  
356 indicative of a nearly pure microbial origin ([e.g. Bernard et al., 1976](#)). This observation may in turn  
357 suggest that microbial methane in deep biosphere do necessarily resemble laboratory cultures ([e.g.](#)  
358 [Wang et al., 2015](#); [Stolper et al., 2015](#); [Douglas et al., 2016](#); [Giunta et al., 2019](#)).

359 Gases from the Western High (DV02-PE01 and PE02) identified as mainly thermogenic also  
360 have disequilibrium  $\Delta^{13}\text{CH}_3\text{D}$  and  $\Delta^{12}\text{CH}_2\text{D}_2$  values (Fig. 3b.) while showing little evidence of a  
361 microbial contribution (low  $C_1/C_{2+}$  of  $\sim 15$ ). Therefore, thermogenic gases may also have contributed to  
362 disequilibrium  $\Delta^{13}\text{CH}_3\text{D}$  and  $\Delta^{12}\text{CH}_2\text{D}_2$  values in mixtures. Deciphering the impact of mixing is  
363 exacerbated by a lack of correlation between  $C_1/C_{2+}$  and disequilibrium isotopologue signatures (Fig 5).  
364 In any event, the  $\Delta^{13}\text{CH}_3\text{D}$  and  $\Delta^{12}\text{CH}_2\text{D}_2$  data from the SoM fail to follow a simple two-component



365 mixing in which thermogenic gases with low  $C_1/C_{2+}$  ratios are mixed with microbial gases with  
366 elevated  $C_1/C_{2+}$  ratios. Mixing does not seem to be the primary cause of variable mass-18 isotopologues  
367 in these samples.

368

### 369 5.2.2 Mass-dependent fractionation during migration

370 An alternative explanation for the disequilibrium trend of highly variable  $\Delta^{13}\text{CH}_3\text{D}$  values and  
371 relatively minor variations in  $\Delta^{12}\text{CH}_2\text{D}_2$  is mass fractionation of the SoM gases during their migration  
372 in the subsurface (i.e. for example from source rock to reservoir or from reservoir to reservoir) and/or  
373 to the seafloor. Though migration of free gas (bubbles) to the seafloor is an advective process and is  
374 therefore not a mechanism for fractionating isotopologues, diffusive transport prior to gas saturation  
375 can segregate methane molecules according to their masses. Diffusion favors the light isotopologues  
376 for the diffused gas (as opposed to the residual gas) resulting in decreases in  $\delta^{13}\text{C}$  and  $\delta\text{D}$  values but  
377 increases in  $\delta^{13}\text{CH}_3\text{D}$  and  $\delta^{12}\text{CH}_2\text{D}_2$  values. In  $\Delta^{12}\text{CH}_2\text{D}_2$  vs.  $\Delta^{13}\text{CH}_3\text{D}$  space both axes refer to the same  
378 integer mass ratio of 18/16, and any fractionation by molecular mass, including by diffusion, should  
379 produce a 1:1 slope in this space (Young et al., 2017). A 1:1 relationship is also expected for gases  
380 affected by diffusion in  $\delta\text{D}$  vs.  $\delta^{13}\text{C}$  space since both axes refer to integer mass ratios of 17/16. In the  
381 SoM gas samples, the slope-1 relationship expected between  $\delta^{13}\text{C}$  and  $\delta\text{D}$  values by mass segregation  
382 according to molecular weight is only crudely evident when taken in aggregate (Fig. 6a). However, the  
383 data are more consistent with a diffusive fractionation process if one considers that  $\Delta^{13}\text{CH}_3\text{D}$  and  
384  $\Delta^{12}\text{CH}_2\text{D}_2$  are distributed along two distinct diffusion trends starting from two equilibrium temperatures  
385 of about ~100 and 200 °C (Fig. 6b). These temperatures are at the high-temperature ends of the two  
386 groups of samples shown in Fig. 3b.

387 If diffusion is at play, samples showing the largest offset from the equilibrium curve in mass-18  
388 isotopologue space should be relatively low in bulk  $\delta^{13}\text{C}$  and  $\delta\text{D}$ . In detail however, when assigning

389 self-consistent diffusion coefficients to all methane isotopologues, it appears that an enrichment of  
390  $> 3 \text{ ‰}$  in  $\Delta^{13}\text{CH}_3\text{D}$  as observed in our data should be associated with a shift in bulk  $\delta^{13}\text{C}$  by  $\sim -50 \text{ ‰}$   
391 (Fig. 6c). This is not observed; our entire suite of data do not range over more than  $\sim 25 \text{ ‰}$  in  $\delta^{13}\text{C}$ , so  
392 that the overall observed range of variations in  $\Delta^{13}\text{CH}_3\text{D}$  appears intrinsically inconsistent with  
393 diffusion (or any mass-dependent process) being a dominant mechanism at play in the subsurface of the  
394 SoM. We conclude that diffusion is not a principal mechanism affecting the mass-18 isotopologue  
395 abundances in our methane samples.

396

### 397 *5.2.3 Microbial methane oxidation*

398 Apparent temperatures inferred from  $\Delta^{13}\text{CH}_3\text{D}$  range from  $131_{-7}^{+6} \text{ °C}$  (DV03-PE03) to  $9_{-3}^{+3} \text{ °C}$  (DV03-  
399 PE09), perhaps representing a range from a deep reservoir temperature to a near seafloor temperature  
400 ( $\sim 14 \text{ °C}$ ) if taken at face value. Thus, one may speculate that venting gases had their  $\Delta^{13}\text{CH}_3\text{D}$  values  
401 re-equilibrated during their ascent towards a near-seafloor temperature, without significantly re-  
402 equilibrating  $\Delta^{12}\text{CH}_2\text{D}_2$  values. Several recent studies have stressed the potential importance of  
403 microbial Anaerobic Methane Oxidation (AOM) in re-ordering isotopic bond associations in methane  
404 gas, and thus causing methane to progressively evolve towards equilibrium at ambient temperatures for  
405 both mass-18 isotopologues (e.g. Young et al., 2017; Giunta et al., 2019; Ash et al., 2019). The uptake  
406 of methane by methanotrophic organisms, in particular by archeal strains performing AOM, is a  
407 widespread process generally occurring in the first few meters of marine sediments, thus at a  
408 temperature that should not be drastically different from those at the seafloor. AOM has been  
409 recognized as a major methane sink in sediments from the SoM (e.g. Crémière et al., 2012), including  
410 in those surrounding the gas seeps studied here (Teichert et al., 2018). However, our samples were all  
411 collected as free-gas (i.e. bubbles), which is generally considered non-accessible to AOM (Luff and  
412 Wallmann 2003; Treude et al., 2003). For AOM to have impacted the gas studied here, it would be

413 required to have occurred prior to gas saturation. AOM is expected to yield a progressive enrichment of  
414 both  $\delta^{13}\text{C}$  and  $\delta\text{D}$  in the residual methane (e.g. Whiticar, 1999; Holler et al., 2011), however there is no  
415 specific relationship between off-equilibrium signature and bulk signatures in our data-set (Fig. 6c may  
416 illustrate that too). In marine sediments however, AOM is expected to occur with significant  
417 reversibility effects (e.g. Yoshinaga et al., 2014), perhaps implying that a classic kinetic framework is  
418 not relevant for this type of settings. The study of methane in shallow sediments from the Bornholm  
419 Basin, Baltic Sea, yielded showed evidence for re-equilibration in  $\Delta^{13}\text{CH}_3\text{D}$  and  $\Delta^{12}\text{CH}_2\text{D}_2$  to  
420 environmental temperature with little effects on the bulk  $\delta^{13}\text{C}$  and  $\delta\text{D}$  signatures (Ash et al., (2019)).  
421 This study suggests that shifts in  $\Delta^{13}\text{CH}_3\text{D}$  and not  $\Delta^{12}\text{CH}_2\text{D}_2$ , as observed in our data, being the result  
422 of AOM is unlikely.

423 A caveat to this conclusion arises because of preliminary experimental results suggesting that  
424 AOM under a set of restrictive conditions may yield signatures similar to our disequilibrated samples  
425 (Young, 2019). These preliminary results suggest that under low sulfate content ( $< 1 \text{ mM}$ ), AOM  
426 mediation would re-equilibrate  $\Delta^{13}\text{CH}_3\text{D}$  to environmental temperatures while maintaining the  
427  $\Delta^{12}\text{CH}_2\text{D}_2$  virtually unchanged. It is unclear how these results may be extrapolated to marine settings,  
428 but the similarity with our data-set suggests that effects on methane isotopologues due to AOM cannot  
429 be ruled out entirely. We note that the presence of a largely  $\Delta^{13}\text{CH}_3\text{D}$  AOM effect driving equilibration  
430 towards colder temperatures would not be inconsistent with non-enzymatic re-equilibration as  
431 described above. The AOM would simply modify the isotopologue abundances equilibrated at  $\sim 90$  and  
432  $\sim 130$  °C, prior to AOM.

433

#### 434 5.2.4. *Different re-equilibration rates for $\Delta^{13}\text{CH}_3\text{D}$ and $\Delta^{12}\text{CH}_2\text{D}_2$ ?*

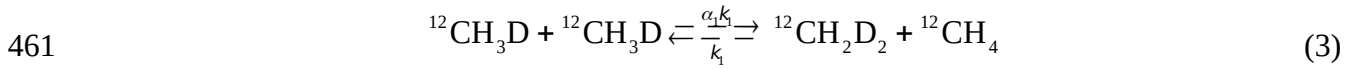
435 In the above sections we have discussed two mechanisms that could cause re-equilibration of  
436 methane isotopologue abundances. We suggested that non-enzymatic (i.e. abiotic) intra-methane

437 exchange could cause re-equilibration of microbial (and perhaps thermogenic) gases formed at low  
438 temperatures to higher temperatures characteristic of known temperatures reached during sediment  
439 burial in the area (section 5.1). The bi-modal distribution of  $\Delta^{12}\text{CH}_2\text{D}_2$  values suggests re-equilibration  
440 to two distinct temperatures of  $\sim 152^\circ\text{C}$  and  $\sim 90^\circ\text{C}$  that appear consistent with the thermal history of  
441 sediments beneath the SoM. Enzymatic (i.e. biotic) facilitated exchange of isotopes among methane gas  
442 molecules could have caused  $\Delta^{13}\text{CH}_3\text{D}$  to partially re-equilibrate to near seafloor temperatures, perhaps  
443 during gas ascent to the seafloor (section 5.2.3). As discussed before, the bi-modal distribution of  
444  $\Delta^{12}\text{CH}_2\text{D}_2$  data seem to point towards two distinct temperatures of  $\sim 152^\circ\text{C}$  and  $\sim 90^\circ\text{C}$  that appear  
445 consistent with the thermal history of sediments beneath the SoM. The variable  $\delta^{13}\text{CH}_3\text{D}$  data span a  
446 range of apparent temperatures from  $\sim 130^\circ\text{C}$  to  $\sim 10^\circ\text{C}$ . Based on these observations, one may  
447 speculate that our data illustrate that re-equilibration rates for the relative abundances of  $^{13}\text{CH}_3\text{D}$  and  
448  $^{12}\text{CH}_2\text{D}_2$  may be different.

449 More specifically, the bi-modal  $\Delta^{12}\text{CH}_2\text{D}_2$  values at two geologically plausible temperatures  
450 suggest isotopic bond re-ordering to equilibrium or near-equilibrium values, while  $\Delta^{13}\text{CH}_3\text{D}$  values are  
451 are more variable, perhaps as a result of only partial re-equilibration. This would imply that  $\Delta^{12}\text{CH}_2\text{D}_2$   
452 re-equilibrates faster than  $\Delta^{13}\text{CH}_3\text{D}$ , and that  $\Delta^{13}\text{CH}_3\text{D}$  carries a memory of pre-reset conditions. Note  
453 this scenario does not allow the microbial methane, prior to re-equilibration, to be as low in  $\Delta^{13}\text{CH}_3\text{D}$  as  
454 observed in culture studies ( $< 4\text{‰}$ ; e.g. [Young et al., 2017](#)) and would rather suggest a microbial  
455 methane (prior re-equilibration) with  $\Delta^{13}\text{CH}_3\text{D} \sim 6\text{‰}$  (equivalent to  $T \sim 15^\circ\text{C}$ ), consistent with the idea  
456 of a deep biosphere methane being nearly equilibrated with environmental temperatures in  $\Delta^{13}\text{CH}_3\text{D}$ .

457 In order to explain our data as being purely the result of different rates of equilibration for  
458  $^{12}\text{CH}_2\text{D}_2$  and  $^{13}\text{CH}_3\text{D}$ , we use a simple kinetic model for exchange. In this model, we consider the intra-  
459 methane exchange reaction:

460



462

463 where  $\alpha_1$  is the equilibrium fractionation factor and  $k_1$  is the rate constant. A simple rate equation for  
464 this reaction is

465

466 
$$\frac{d[^{12}\text{CH}_2\text{D}_2]}{dt} = \alpha_1 k_1 [^{12}\text{CH}_3\text{D}]^2 - k_1 [^{12}\text{CH}_2\text{D}_2] [^{12}\text{CH}_4] \quad (4)$$

467

468 For simplification, the concentration of  $^{12}\text{CH}_4$  is set to unity ( $[^{12}\text{CH}_4] = 1$ ), making what follows all  
469 relative to  $^{12}\text{CH}_4$ . We also invoke the approximation that  $\alpha_1 k_1 [^{12}\text{CH}_3\text{D}]^2$  is a constant. This is justified  
470 since the concentration of  $^{12}\text{CH}_2\text{D}_2$  relative to  $\text{CH}_4$  is about  $10^{-8}$  while that of  $^{12}\text{CH}_3\text{D}$  is  $10^{-4}$ , so  
471  $[^{12}\text{CH}_3\text{D}] \gg [^{12}\text{CH}_2\text{D}_2]$  even when working at the per mil level. In other words, we treat the change in  
472 the  $[^{12}\text{CH}_2\text{D}_2]/[^{12}\text{CH}_4]$  ratio as a change in  $[^{12}\text{CH}_2\text{D}_2]$  only in the rate equation. With this approximation,  
473 and some rearrangements, one obtains the solution to the differential equation as being

474

475 
$$[^{12}\text{CH}_2\text{D}_2]_t = [^{12}\text{CH}_2\text{D}_2]_{\text{EQ}} + \left\{ [^{12}\text{CH}_2\text{D}_2]_o - [^{12}\text{CH}_2\text{D}_2]_{\text{EQ}} \right\} e^{-k_1 t} \quad (5)$$

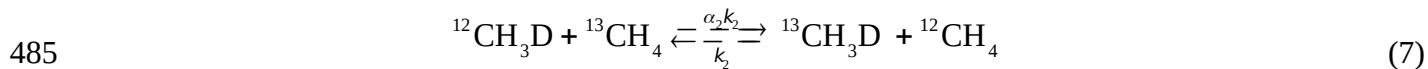
476

477

478 where  $t$  is the time of the observation, the EQ subscript indicates equilibrium, and the o subscript  
479 indicates the initial value. Notice that as  $t \rightarrow \infty$ , Equation (x) reduces to  $[^{12}\text{CH}_2\text{D}_2]_t = [^{12}\text{CH}_2\text{D}_2]_{\text{EQ}}$ . This  
480 equation can be further rearranged into a more convenient form by dividing through by the equilibrium  
481 concentration of  $\text{CH}_2\text{D}_2$ , yielding

482 
$$\frac{[^{12}\text{CH}_2\text{D}_2]_t - [^{12}\text{CH}_2\text{D}_2]_{\text{EQ}}}{[^{12}\text{CH}_2\text{D}_2]_o - [^{12}\text{CH}_2\text{D}_2]_{\text{EQ}}} = e^{-k_1 t} \quad (6)$$

483 The left-hand side of Equation (x) is the fractional approach to equilibrium. The analogous exchange  
484 reaction for  $^{13}\text{CH}_3\text{D}$  is



486

487 and results in

$$488 \quad \frac{[^{13}\text{CH}_3\text{D}]_t - [^{13}\text{CH}_3\text{D}]_{\text{EQ}}}{[^{13}\text{CH}_3\text{D}]_0 - [^{13}\text{CH}_3\text{D}]_{\text{EQ}}} = e^{-k_2 t} \quad (8)$$

489 The form of Equations (7) and (8) show that if the rate constants are the same, and so the e-folding  
490 times being  $\tau_i = 1/k_i$  are the same, then the relative rates of equilibration depend on the degree of  
491 disequilibrium. For example, for an initial gas  $-50\text{‰}$  out of equilibrium in  $\Delta^{12}\text{CH}_2\text{D}_2$  and  $-2\text{‰}$  out of  
492 equilibrium in  $^{13}\text{CH}_3\text{D}$ , after  $t = 2\tau$ , we obtain  $\Delta^{12}\text{CH}_2\text{D}_2 = -7\text{‰}$  relative to equilibrium (a total shift of  
493  $+43\text{‰}$ ) and  $^{13}\text{CH}_3\text{D}$  is  $-0.3\text{‰}$  relative to equilibrium (a total shift of  $+1.6\text{‰}$ ). So, if the rate constants  
494 for D/H exchange, for example, are the same for the two isotopologues, we should see much larger  
495 shifts in  $^{12}\text{CH}_2\text{D}_2$  relative to those in  $^{13}\text{CH}_3\text{D}$ , but, when the former is at equilibrium, the latter should be  
496 also.

497 We find that unequal rate constants are required to explain our data if the methane prior to re-  
498 equilibration was in equilibrium at the lower temperatures suggested by the highest  $\Delta^{13}\text{CH}_3\text{D}$  values.  
499 Indeed, for such initial conditions, we calculate that the rate for re-equilibrating  $\Delta^{12}\text{CH}_2\text{D}_2$  would have  
500 to be 5 to 10 times that of  $\Delta^{13}\text{CH}_3\text{D}$  to explain a nearly-horizontal relationship as observed in Figure 7.  
501 Whether such large difference of re-equilibration rates between the two isotopologues is likely or not  
502 will have to be explored in future experimental work. However, based on an analysis of the rates of  
503 equilibration based on the symmetry numbers for reactants and transition states (see [Labidi et al., 2020](#)  
504 and Supplementary material), we conclude that one should not expect  $k_1/k_2$  (i.e., the rate constant for  
505  $^{12}\text{CH}_2\text{D}_2$  relative to that for  $^{13}\text{CH}_3\text{D}$ ) to be not larger than 2. With this constraint, fitting the SoM data

506 suggests that the initial mass-18 isotopologue composition was below the equilibrium curve (Fig. 7).  
507 An initial composition such as this for a microbial gas is not unreasonable given the propensity of  
508 microbial methanogenesis to produce low  $\Delta^{12}\text{CH}_2\text{D}_2$  values in general, even in some marine  
509 environments (e.g., [Ash et al., 2019](#)).

510

#### 511 *6. Implications for the use of methane isotopologues as geothermometers*

512 Three pathways for methane generation (abiotic, thermogenic and microbial) are generally  
513 expected to be controlled by kinetic effects rather than by thermodynamic equilibrium. It is thus  
514 remarkable that in many instances in nature, especially for thermogenic gases, the ‘clumped’  
515 composition appears consistent with bond equilibrium. Hence, assessing whether such equilibrium is  
516 inherited: 1) from the formation of the methane itself; or 2) from isotopic bond-order re-equilibration  
517 under conditions and timescales that remain to be defined, is critical for understanding the true meaning  
518 of ‘clumped’-based temperatures. In the first case, the ‘clumped’ composition may accurately record  
519 the formation temperature of the methane, whereas in the second case, it is overprinted by a re-  
520 equilibration temperature experienced at a point in time in the thermal history of the gas.

521 We suggest that pristine  $\Delta^{13}\text{CH}_3\text{D}$  and  $\Delta^{12}\text{CH}_2\text{D}_2$  signatures inherited from methane generation,  
522 in particular of microbial methanogenesis, have been fully or partially overprinted by re-equilibration  
523 within the subsurface of the SoM. This conclusion thus supports the idea that in sedimentary reservoirs,  
524 isotopologue equilibrium might sometimes be reached after  $\text{CH}_4$  formation. The timescales for re-  
525 equilibration remain to be established. Though these rates certainly depend on the associated  
526 mineralogy as well as on the presence of H-bearing molecules, they likely scale with temperature  
527 ([Stolper et al., 2017](#)). This suggests that ‘clumped’-based temperatures are more prone to record the  
528 highest temperatures experienced by the gases. Considering that thermogenic gases are formed  
529 continuously during burial, thus spanning a wide range of temperatures, methane formed at lower

530 temperatures eventually re-equilibrates to the highest temperature reached. This hypothesis would  
531 explain why temperatures derived from ‘clumped’ isotopologues for thermogenic gases often match the  
532 maximum burial temperatures (Stolper et al., 2014, 2017).

533 On the other hand, data from sedimentary reservoirs in Southwest Ontario and Michigan basins  
534 (Giunta et al., 2019) show considerable  $\Delta^{12}\text{CH}_2\text{D}_2$  disequilibrium, illustrating a mixing relationship  
535 between thermogenic and microbial methane (see Fig. 4). Those disequilibrium signatures are similar  
536 to those observed in laboratory cultures, and suggests that re-equilibration in these reservoirs was  
537 limited (if any), thus contrasting with the Marmara system studied here. A possible explanation is that  
538 samples from Southwest Ontario and Michigan basins come from sedimentary units that never  
539 experienced temperatures greater 40-50 °C. We thus speculate that an activation temperature exist,  
540 below which rates for re-equilibration are too slow for significant effects on  $\Delta^{13}\text{CH}_3\text{D}$  and  $\Delta^{12}\text{CH}_2\text{D}_2$   
541 over geological timescales. Identifying threshold temperatures would help define where to expect re-  
542 equilibration of microbial methane that is generally formed at lower temperatures than thermogenic  
543 gases. From our data, isotopologue equilibrium measured for samples of apparent microbial origin,  
544 samples DV05-PE02, DV04-PE04 and PE08, indicates that re-equilibration to temperatures down to  
545 90 °C likely occurs. Notwithstanding that re-equilibration rates are likely a function of *in situ* chemical  
546 and mineralogical conditions, the contrasting results of these two studies may in turn suggest that a  
547 temperature of 40-50 °C is not sufficient for significant re-equilibration of methane isotopic bond  
548 ordering.

549

## 550 **5/ Conclusion**

551 We measured  $\Delta^{13}\text{CH}_3\text{D}$  and  $\Delta^{12}\text{CH}_2\text{D}_2$  from methane-rich cold seeps emanating at the seafloor  
552 of the sea of Marmara (SoM). The variability observed among the samples further demonstrates the  
553 occurrence of a multitude of distinct gas reservoirs in the subsurface of the SoM, which is consistent



554 with previous observations based on gas geochemistry (Ruffine et al., 2018b), as well as on seismic  
555 imaging (Geli et al., 2018).

556 Although  $\Delta^{13}\text{CH}_3\text{D}$  and  $\Delta^{12}\text{CH}_2\text{D}_2$  have been recently used to infer the dominant production  
557 mechanism (including sometimes, formation temperature) or mixing relationship between different  
558 sources of methane (e.g. Giunta et al., 2019), here we show that methane isotopologues signatures in  
559 the SoM cannot be simply explained by mixing. Instead, methane effusing from the SoM seafloor  
560 appear to be affected, to varying degrees, by bond re-equilibration, a process in which the isotope  
561 bond-ordering inherited from the formation of the methane is subsequently ‘re-set’ to thermodynamic  
562 equilibrium during residence at sufficiently high temperatures. This conclusion may suggest that  
563 apparent isotopologue equilibrium like overwhelmingly displayed among thermogenic gases (Stolper et  
564 al., 2014, 2015, 2017; Wang et al., 2015; Young et al., 2017; Giunta et al., 2019) can in some cases be  
565 acquired after formation and therefore, that isotopologue apparent temperatures may trace re-  
566 equilibration temperatures rather than the actual formation temperature.

567

## 568 **Acknowledgments**

569 We thank the captain and his crew on-board the RV *Pourquoi pas?* This study was supported by  
570 fundings from the European programme “MARsite” under the call ENV.2012.6.4-2, as well as by  
571 LabexMER (ANR-10-LABX-19) through the project MicroGaMa. The authors wish to thank Nina  
572 Tanguy for providing the bathymetric map. They also thank Dr. David T. Wang, one anonymous  
573 reviewer and Dr. Laura Robinson for their helpful comments.

574

575

576

577

578 **Appendices**

579 **Isotopologue relationship to temperature**

580 The relationship between  $\Delta^{13}\text{CH}_3\text{D}$  and  $\Delta^{12}\text{CH}_2\text{D}_2$  and temperature can be predicted through *ab initio*  
581 calculations (e.g. [Ma et al., 2008](#); [Webb and Miller, 2014](#); [Liu and Liu, 2016](#)). In this study, we used the  
582 recent expressions proposed by [Young et al., \(2016, 2017\)](#):

583  
584 
$$\Delta^{13}\text{CH}_3\text{D} (T) \approx 1000 \ln (1 + 0.0355502/T - 433.038/T^2 + 1270210.0/T^3 - 5.94804 \times 10^8/T^4 + 1.196630$$
  
585 
$$\times 10^{11}/T^5 - 9.07230 \times 10^{12}/T^6)$$
 A.1

586  
587 and

588  
589 
$$\Delta^{12}\text{CH}_2\text{D}_2 (T) \approx 1000 \ln (1 + 0.183798/T - 785.483/T^2 + 1056280.0/T^3 + 9.37307 \times 10^7/T^4 - 8.919480 \times$$
  
590 
$$10^{10}/T^5 + 9.901730 \times 10^{12}/T^6)$$
 A.2

591  
592 where T is in Kelvin. The differences between the different computational methods to predict  
593 relationship between  $\Delta$  values and temperatures are less than the analytical uncertainties ([Webb and](#)  
594 [Miller, 2014](#); [Liu and Liu, 2016](#), [Young et al., 2017](#)).

595  
596  
597  
598  
599  
600  
601  
602  
603  
604  
605  
606  
607  
608  
609  
610  
611  
612  
613  
614  
615  
616  
617  
618  
619  
620  
621

## 622 **References**

- 623 Alexander, R., Kagi, R. I., & Larcher, A. V. (1982). Clay catalysis of aromatic hydrogen-exchange reactions. *Geochimica et*  
624 *Cosmochimica Acta*, 46(2), 219-222.
- 625
- 626 Ambraseys, N. N., & Jackson, J. A. (2000). Seismicity of the Sea of Marmara (Turkey) since 1500. *Geophysical Journal*  
627 *International*, 141(3), F1-F6.
- 628
- 629 Armijo, R., Meyer, B., Barka, A., de Chabalier, J. B., Hubert-Ferrari, A., & Cakir, Z. (2000). The fault breaks of the 1999  
630 earthquakes in Turkey and the tectonic evolution of the Sea of Marmara: a summary. *The 1999 İzmit and Düzce*  
631 *earthquakes: preliminary results*, 55-62.
- 632
- 633 Ash, J., Egger, M., Treude, T., Kohl, I., Cragg, B., Parkes, R. J., ... & Young, E. D. (2019). Exchange catalysis during  
634 anaerobic methanotrophy revealed by 12CH<sub>2</sub>D<sub>2</sub> and 13CH<sub>3</sub>D in methane. *Geochemical Perspective Letters*, 10, 26-30.
- 635
- 636 Bernard, B. B., Brooks, J. M., & Sackett, W. M. (1976). Natural gas seepage in the Gulf of Mexico. *Earth and Planetary*  
637 *Science Letters*, 31(1), 48-54.
- 638
- 639 Berner, U., and Faber, E., 1996, Empirical carbon isotope/maturity relationships for gases from algal kerogens and  
640 terrigenous organic matter, based on dry, open-system pyrolysis: *Organic Geochemistry*, v. 24, no. 10-11, p. 947-955.
- 641
- 642 Bourry, C., Chazallon, B., Charlou, J. L., Donval, J. P., Ruffine, L., Henry, P., ... & Moreau, M. (2009). Free gas and gas  
643 hydrates from the Sea of Marmara, Turkey: Chemical and structural characterization. *Chemical Geology*, 264(1-4), 197-206.
- 644
- 645 Çağatay, M. N., Yıldız, G., Bayon, G., Ruffine, L., and Henry, P., 2018, Seafloor authigenic carbonate crusts along the  
646 submerged part of the North Anatolian Fault in the Sea of Marmara: Mineralogy, geochemistry, textures and genesis: *Deep*  
647 *Sea Research Part II: Topical Studies in Oceanography*.
- 648
- 649 Cao, X., Bao, H., & Peng, Y. (2019). A kinetic model for isotopologue signatures of methane generated by biotic and abiotic  
650 CO<sub>2</sub> methanation. *Geochimica et Cosmochimica Acta*, 249, 59-75.
- 651 Clayton, C. (1991). Carbon isotope fractionation during natural gas generation from kerogen. *Marine and petroleum*  
652 *geology*, 8(2), 232-240.
- 653
- 654 Crémière, A., Pierre, C., Blanc-Valleron, M. M., Zitter, T., Çağatay, M. N., & Henry, P. (2012). Methane-derived authigenic  
655 carbonates along the North Anatolian fault system in the Sea of Marmara (Turkey). *Deep Sea Research Part I:*  
656 *Oceanographic Research Papers*, 66, 114-130.
- 657
- 658 Douglas, P. M. J., Stolper, D. A., Smith, D. A., Anthony, K. W., Paull, C. K., Dallimore, S., ... & Sessions, A. L. (2016).  
659 Diverse origins of Arctic and Subarctic methane point source emissions identified with multiply-substituted isotopologues.  
660 *Geochimica et Cosmochimica Acta*, 188, 163-188.
- 661
- 662 Eldridge, D. L., Korol, R., Lloyd, M. K., Turner, A. C., Webb, M. A., Miller, T. F., & Stolper, D. (2019). Comparison of  
663 Experimental vs. Theoretical Abundances of 13CH<sub>3</sub>D and 12CH<sub>2</sub>D<sub>2</sub> for Isotopically Equilibrated Systems From 1-500° C.  
664 *ACS Earth and Space Chemistry*.
- 665
- 666 Gasperini, L., Polonia, A., Bortoluzzi, G., Henry, P., Le Pichon, X., Tryon, M., Çağatay, N., and Geli, L., 2011, How far did  
667 the surface rupture of the 1999 İzmit earthquake reach in Sea of Marmara?: *Tectonics*, v. 30.
- 668
- 669 Géli, L., Henry, P., Zitter, T., Dupré, S., Tryon, M., Çağatay, M. N., ... & Natalin, B. (2008). Gas emissions and active  
670 tectonics within the submerged section of the North Anatolian Fault zone in the Sea of Marmara. *Earth and Planetary*  
671 *Science Letters*, 274(1-2), 34-39.

672  
673 Géli, L., Henry, P., Grall, C., Tary, J. B., Lomax, A., Batsi, E., ... & Sengör, A. M. C. (2018). Gas and seismicity within the  
674 Istanbul seismic gap. *Scientific reports*, 8(1), 6819.  
675  
676 Giunta, T., Young, E. D., Warr, O., Kohl, I., Ash, J. L., Martini, A., ... & LaRowe, D. E. (2019). Methane sources and sinks  
677 in continental sedimentary systems: New insights from paired clumped isotopologues  $^{13}\text{CH}_3\text{D}$  and  $^{12}\text{CH}_2\text{D}_2$ . *Geochimica*  
678 *et Cosmochimica Acta*, 245, 327-351.  
679  
680 Gonzalez, Y., Nelson, D.D., Shorter, J.H., McManus, J.B., Dyroff, C., Formolo, M., Wang, D.T., Western, C.M. and Ono, S.,  
681 2019. Precise measurements of  $^{12}\text{CH}_2\text{D}_2$  by tunable infrared laser direct absorption spectroscopy. *Analytical Chemistry*,  
682 91(23), pp.14967-14974.  
683  
684 Gruen, D. S., Wang, D. T., Könneke, M., Topçuoğlu, B. D., Stewart, L. C., Goldhammer, T., ... & Ono, S. (2018).  
685 Experimental investigation on the controls of clumped isotopologue and hydrogen isotope ratios in microbial methane.  
686 *Geochimica et Cosmochimica Acta*, 237, 339-356.  
687  
688 Gürgey, K., Philp, R., Clayton, C., Emiro lu, H., and Siyako, M., 2005, Geochemical and isotopic approach to  
689 maturity/source/mixing estimations for natural gas and associated condensates in the Thrace Basin, NW Turkey: Applied  
690 Geochemistry, v. 20, no. 11, p. 2017-2037.  
691  
692 Gürgey, K. (2009). Geochemical overview and undiscovered gas resources generated from Hamitabat petroleum system in  
693 the Thrace Basin, Turkey. *Marine and Petroleum Geology*, 26(7), 1240-1254.  
694  
695 Head, I. M., Jones, D. M., & Larter, S. R. (2003). Biological activity in the deep subsurface and the origin of heavy oil.  
696 *Nature*, 426(6964), 344.  
697  
698 Holler, T., Widdel, F., Knittel, K., Amann, R., Kellermann, M. Y., Hinrichs, K. U., ... & Wegener, G. (2011). Thermophilic  
699 anaerobic oxidation of methane by marine microbial consortia. *The ISME journal*, 5(12), 1946-1956.  
700  
701 Inagaki, F., Hinrichs, K. U., Kubo, Y., Bowles, M. W., Heuer, V. B., Hong, W. L., ... & Kaneko, M. (2015). Exploring deep  
702 microbial life in coal-bearing sediment down to ~ 2.5 km below the ocean floor. *Science*, 349(6246), 420-424.  
703  
704 James, A.T. and Burns, B.J., 1984. Microbial alteration of subsurface natural gas accumulations. AAPG Bulletin, 68(8),  
705 pp.957-960.  
706  
707 Kashafi, K., & Lovley, D. R. (2003). Extending the upper temperature limit for life. *Science*, 301(5635), 934-934.  
708  
709 Labidi, J., Young, E. D., Giunta, T., Kohl, I. E., Seewald, J., Tang, H., ... & Früh-Green, G. L. (2020). Methane thermometry  
710 in deep-sea hydrothermal systems: evidence for re-ordering of doubly-substituted isotopologues during fluid cooling.  
711 *Geochimica et Cosmochimica Acta*.  
712  
713 Luff, R., & Wallmann, K. (2003). Fluid flow, methane fluxes, carbonate precipitation and biogeochemical turnover in gas  
714 hydrate-bearing sediments at Hydrate Ridge, Cascadia Margin: numerical modeling and mass balances. *Geochimica et*  
715 *Cosmochimica Acta*, 67(18), 3403-3421.  
716  
717 Martini, A. M., Walter, L. M., Budai, J. M., Ku, T. C., Kaiser, C. J., & Schoell, M. (1998). Genetic and temporal relations  
718 between formation waters and biogenic methane: Upper Devonian Antrim Shale, Michigan Basin, USA. *Geochimica et*  
719 *Cosmochimica Acta*, 62(10), 1699-1720.  
720

721 Prinzhofer, A., & Pernaton, E. (1997). Isotopically light methane in natural gas: bacterial imprint or diffusive fractionation?.

722 *Chemical Geology*, 142(3-4), 193-200.

723

724 Reeves, E. P., Seewald, J. S., & Sylva, S. P. (2012). Hydrogen isotope exchange between n-alkanes and water under

725 hydrothermal conditions. *Geochimica et Cosmochimica Acta*, 77, 582-599.

726

727 Ruffine, L., Dennielou, B., Giovanni, B., Namik, Ç. M., Grall, C., Jean-Luc, C., ... & Etoubleau, J. (2012). *Geochemical*

728 *dynamics of the natural-gas hydrate system in the Sea of Marmara, offshore Turkey*. INTECH Open Access Publisher.

729

730 Ruffine, L., Ondreas, H., Blanc-Valleron, M. M., Teichert, B. M., Scalabrin, C., Rinnert, E., ... & Donval, J. P. (2018a).

731 Multidisciplinary investigation on cold seeps with vigorous gas emissions in the Sea of Marmara (MarsiteCruise): Strategy

732 for site detection and sampling and first scientific outcome. *Deep Sea Research Part II: Topical Studies in Oceanography*,

733 153, 36-47.

734

735 Ruffine, L., Donval, J. P., Croguennec, C., Burnard, P., Lu, H., Germain, Y., ... & Madre, D. (2018b). Multiple gas reservoirs

736 are responsible for the gas emissions along the Marmara fault network. *Deep Sea Research Part II: Topical Studies in*

737 *Oceanography*, 153, 48-60.

738

739 Ruffine, L., Germain, Y., Polonia, A., de Prunelé, A., Croguennec, C., Donval, J. P., ... & Grall, C. (2015). Pore water

740 geochemistry at two seismogenic areas in the Sea of Marmara. *Geochemistry, Geophysics, Geosystems*, 16(7), 2038-2057.

741

742 Sattler, A. (2018). Hydrogen/Deuterium (H/D) exchange catalysis in alkanes. *ACS Catalysis*, 8(3), 2296-2312.

743

744 Sessions A. L., Sylva S. P., Summons R. E. and Hayes J. M. (2004). Isotopic exchange of carbon-bound hydrogen over

745 geologic timescales. *Geochim. Cosmochim. Acta* 68, 1545–1559

746

747 Schoell, M. (1988). Multiple origins of methane in the Earth. *Chemical geology*, 71(1-3), 1-10.

748

749 Shuai, Y., Douglas, P. M., Zhang, S., Stolper, D. A., Ellis, G. S., Lawson, M., ... & Hu, G. (2018). Equilibrium and non-

750 equilibrium controls on the abundances of clumped isotopologues of methane during thermogenic formation in laboratory

751 experiments: Implications for the chemistry of pyrolysis and the origins of natural gases. *Geochimica et Cosmochimica*

752 *Acta*, 223, 159-174.

753

754 Stolper, D. A., Sessions, A. L., Ferreira, A. A., Neto, E. S., Schimmelmann, A., Shusta, S. S., ... & Eiler, J. M. (2014).

755 Combined 13 C–D and D–D clumping in methane: Methods and preliminary results. *Geochimica et Cosmochimica Acta*,

756 126, 169-191.

757

758 Stolper, D. A., Lawson, M., Davis, C. L., Ferreira, A. A., Neto, E. S., Ellis, G. S., ... & Sessions, A. L. (2014). Formation

759 temperatures of thermogenic and biogenic methane. *Science*, 344(6191), 1500-1503.

760

761 Stolper, D. A., Martini, A. M., Clog, M., Douglas, P. M., Shusta, S. S., Valentine, D. L., ... & Eiler, J. M. (2015).

762 Distinguishing and understanding thermogenic and biogenic sources of methane using multiply substituted isotopologues.

763 *Geochimica et Cosmochimica Acta*, 161, 219-247.

764

765 Stolper, D. A., Lawson, M., Formolo, M. J., Davis, C. L., Douglas, P. M., & Eiler, J. M. (2017). The utility of methane

766 clumped isotopes to constrain the origins of methane in natural gas accumulations. *Geological Society, London, Special*

767 *Publications*, 468, SP468-3.

768

769 Taenzer, L., Labidi, J., Masterson, A. L., Feng, X., Rumble III, D., Young, E. D., & Leavitt, W. D. (2020). Low  $\Delta^{12}\text{CH}_2\text{D}_2$   
770 values in microbialgenic methane result from combinatorial isotope effects. *Geochimica et Cosmochimica Acta*, 285, 225-  
771 236.

772

773 Takai, K., Nakamura, K., Toki, T., Tsunogai, U., Miyazaki, M., Miyazaki, J., ... & Horikoshi, K. (2008). Cell proliferation at  
774 122 C and isotopically heavy  $\text{CH}_4$  production by a hyperthermophilic methanogen under high-pressure cultivation.  
775 *Proceedings of the National Academy of Sciences*, 105(31), 10949-10954.

776

777 Tang, Y., Perry, J. K., Jenden, P. D., & Schoell, M. (2000). Mathematical modeling of stable carbon isotope ratios in natural  
778 gases. *Geochimica et Cosmochimica Acta*, 64(15), 2673-2687.

779

780 Teichert, B. M. A., Chevalier, N., Gussone, N., Bayon, G., Ponzevera, E., Ruffine, L., & Strauss, H. (2018). Sulfate-  
781 dependent anaerobic oxidation of methane at a highly dynamic bubbling site in the Eastern Sea of Marmara (Çınarcık  
782 Basin). *Deep Sea Research Part II: Topical Studies in Oceanography*, 153, 79-91.

783

784 Tissot, B., & Welte, D. H. (1978). Petroleum occurrence and formation.

785

786 Treude, T., Boetius, A., Knittel, K., Wallmann, K., & Jørgensen, B. B. (2003). Anaerobic oxidation of methane above gas  
787 hydrates at Hydrate Ridge, NE Pacific Ocean. *Marine Ecology Progress Series*, 264, 1-14.

788

789 Wang, Z., Schauble, E. A., & Eiler, J. M. (2004). Equilibrium thermodynamics of multiply substituted isotopologues of  
790 molecular gases. *Geochimica et Cosmochimica Acta*, 68(23), 4779-4797.

791

792 Wang, D. T., Gruen, D. S., Sherwood Lollar, B., Hinrichs, K. U., Stewart, L. C., Holden, J. F., ... & Delwiche, K. B. (2015).  
793 Nonequilibrium clumped isotope signals in microbial methane. *Science*, 348(6233), 428-431.

794

795 Wang, D. T., Reeves, E. P., McDermott, J. M., Seewald, J. S., & Ono, S. (2018). Clumped isotopologue constraints on the  
796 origin of methane at seafloor hot springs. *Geochimica et Cosmochimica Acta*, 223, 141-158.

797

798 Whiticar, M. J. (1999). Carbon and hydrogen isotope systematics of bacterial formation and oxidation of methane. *Chemical*  
799 *Geology*, 161(1-3), 291-314.

800

801 Xia, X., & Gao, Y. (2019). Kinetic clumped isotope fractionation during the thermal generation and hydrogen exchange of  
802 methane. *Geochimica et Cosmochimica Acta*, 248, 252-273.

803

804 Yoshinaga, M. Y., Holler, T., Goldhammer, T., Wegener, G., Pohlman, J. W., Brunner, B., ... & Elvert, M. (2014). Carbon  
805 isotope equilibration during sulphate-limited anaerobic oxidation of methane. *Nature Geoscience*, 7(3), 190-194.

806

807 Young, E. D., Rumble III, D., Freedman, P., & Mills, M. (2016). A large-radius high-mass-resolution multiple-collector  
808 isotope ratio mass spectrometer for analysis of rare isotopologues of  $\text{O}_2$ ,  $\text{N}_2$ ,  $\text{CH}_4$  and other gases. *International Journal of*  
809 *Mass Spectrometry*, 401, 1-10.

810

811 Young, E. D., Kohl, I. E., Lollar, B. S., Etiope, G., Rumble Iii, D., Li, S., ... & Sutcliffe, C. (2017). The relative abundances  
812 of resolved  $\text{l}^2\text{CH}_2\text{D}_2$  and  $\text{l}^3\text{CH}_3\text{D}$  and mechanisms controlling isotopic bond ordering in abiotic and biotic methane gases.  
813 *Geochimica et Cosmochimica Acta*, 203, 235-264.

814

815

816

817

818

819 **Table 1:** Data for Marmara gas samples. Isotopologue-based temperatures are calculated based on equations in the  
 820 Appendix. Errors on temperature calculation are  $1\sigma$ .

821

822

823

Location	Sample	Ruffine et al., (2018b)			Measured on the Panorama (this study)							
		$\delta^{13}\text{C}$ (VPDB)	$\delta\text{D}$ (VSMOW)	$\text{C}_1/\text{C}_{2+}$	$\delta^{13}\text{C}$ (VPDB)	$\delta\text{D}$ (VSMOW)	$\Delta^{13}\text{CH}_3\text{D}$	$\text{T}^\circ\text{C}$	$\pm$	$\Delta^{12}\text{CH}_2\text{D}_2$	$\text{T}^\circ\text{C}$	$\pm$
DV1-Central High	DV1-PE02	-43.5	-210	206	-43.3	-207.4	4.59	68.0	4/5	12.00	91.5	9/9
	DV1-PE03	-53	-223	120								
DV2-Western High	DV2-PE01	-44.6	-222	19	-44.6	-220.9	5.00	51.5	4/4	8.47	142	13/15
	DV2-PE02	-44	-229	9	-43.8	-226.1	4.63	66.5	5/5	8.58	140	13/15
DV3-Western flank Tekirdag	DV3-PE01	-52.3	-214	31	-52.0	-212.3	6.06	16.0	3/3	7.08	169.3	16/19
	DV3-PE02	-57.3	-218	34	n.m	n.m	n.m	n.m		n.m	n.m	
	DV3-PE03	-41.9	-173	10	-41.2	-169.7	3.40	130.5	6/7	9.16	130.3	12/14
	DV3-PE04	-54.8	-216	880	-54.6	-214.0	4.41	76.0	5/5	8.21	146.6	14/15
	DV3-PE06	-52.2	-213	31	-51.9	-210.7	3.99	96.5	6/6	5.77	201.5	21/25
DV4-Southeastern flank Tekirdag	DV3-PE09	-58.4	-215	1560	-58.0	-214.2	6.30	9.0	3/3	11.25	100.5	10/11
	DV4-PE02	-63.8	-210	5285	-63.8	-208.1	4.29	81.5	5/6	11.61	96	10/10
	DV4-PE07	-66.1	-237	19505	-65.8	-235.6	5.13	46.5	4/4	12.27	88.2	9/10
DV5-Cinarcik Basin	DV4-PE08	-66	-243	23147	-65.8	-240.8	4.34	79.5	5/5	12.27	88.2	9/10
	DV5-PE01	-63.5	-253	1853	-63.3	-252.2	3.89	102.0	6/6	7.29	164.8	16/18
	DV5-PE02	-63.1	-251	1456	-62.9	-248.5	3.50	124.5	7/7	8.61	139.5	14/15
	DV5-PE03	-63.8	-248	12314	-63.7	-249.2	5.70	27.0	3/3	8.89	134.8	13/14
	DV5-PE04	-62.1	-228	1437	n.m	n.m	n.m	n.m		n.m	n.m	

824

825

826

827

828

829

830

831

832

833

834

835

836

837

838

839

840

841

842

843

844

845

846

847

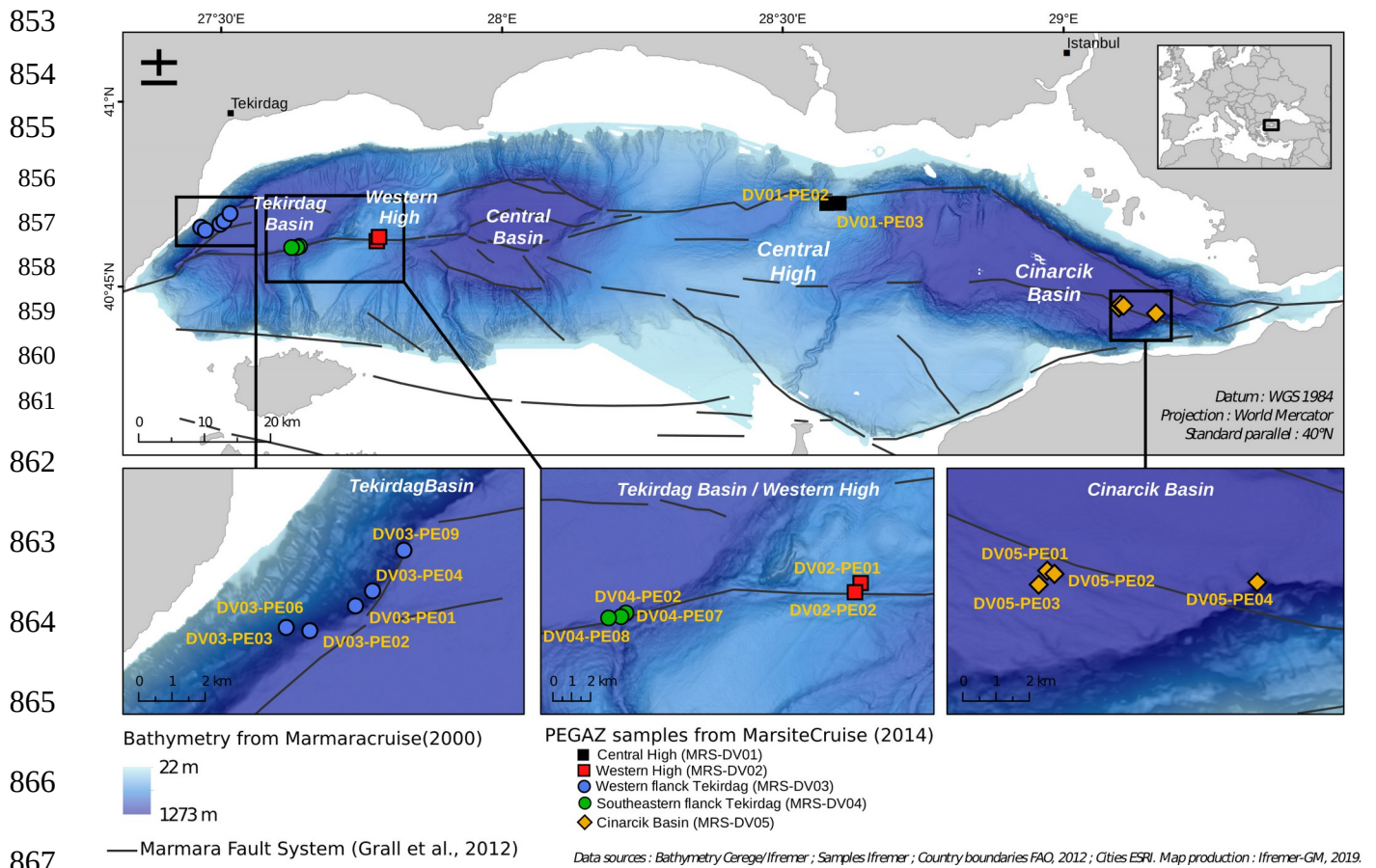
848

849

850

851

852

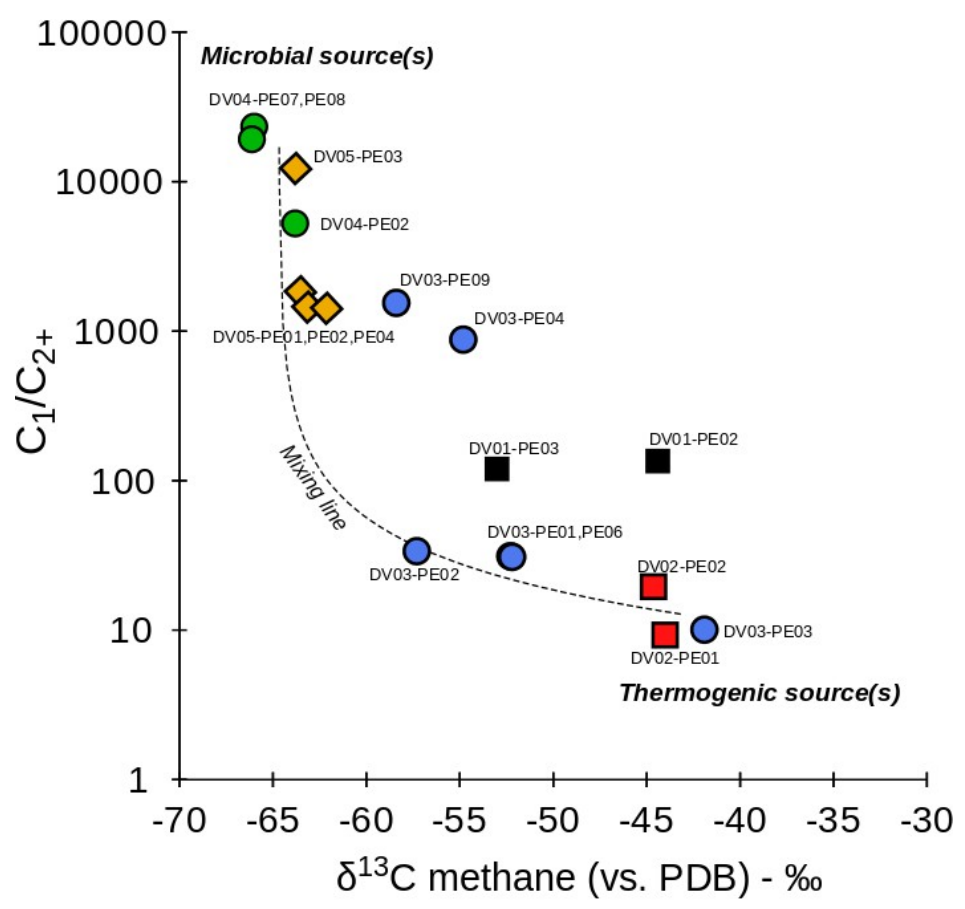


868 **Figure 1:** Map of the sea of Marmara showing the location of the five ROV dives (DV) and gas  
 869 sampling locations.

870  
871  
872  
873  
874  
875  
876  
877  
878  
879  
880  
881  
882

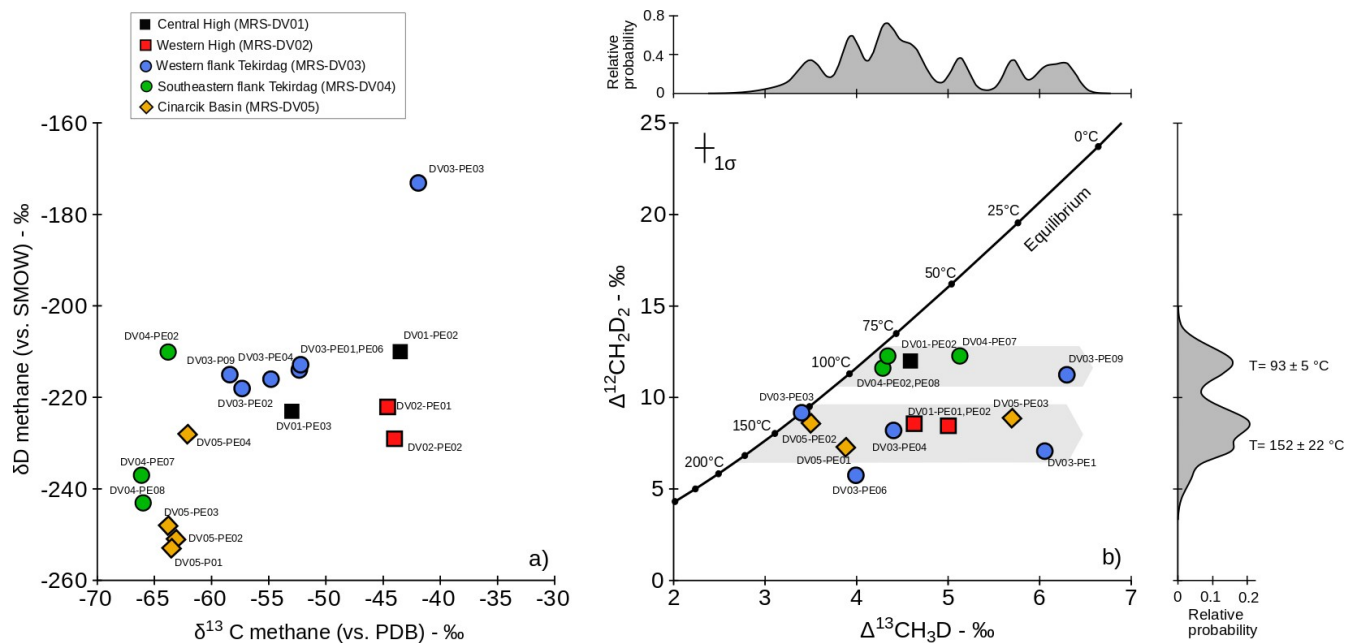


883  
884  
885  
886  
887  
888  
889  
890  
891  
892  
893  
894  
895  
896  
897  
898  
899  
900  
901  
902  
903  
904  
905  
906  
907  
908  
909  
910  
911  
912  
913  
914



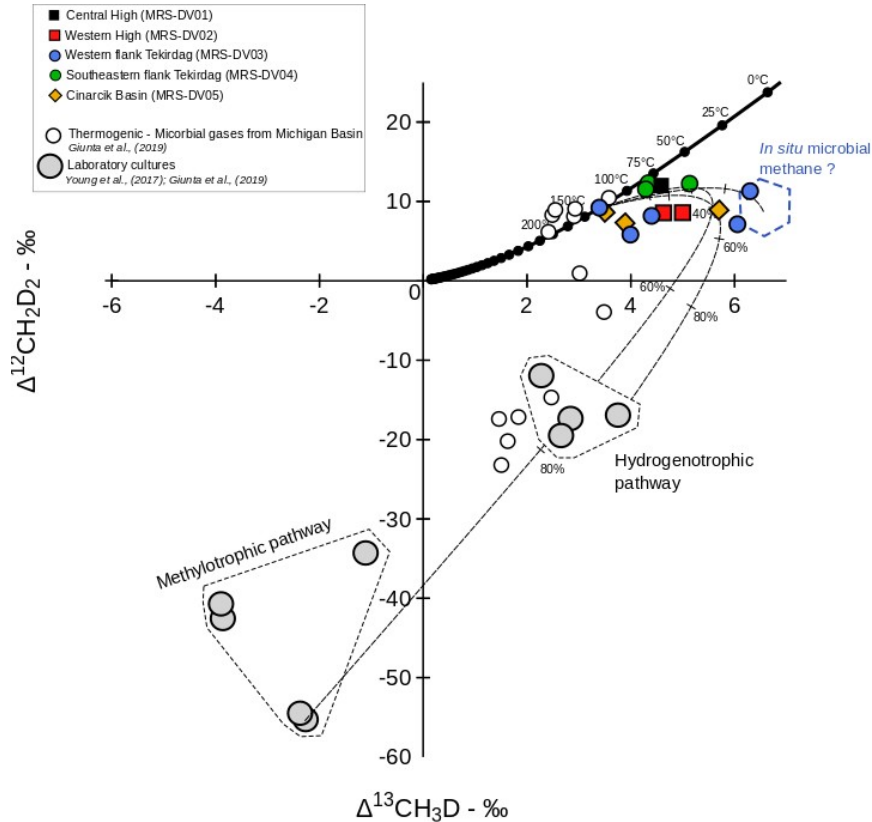
**Figure 2:** ‘Bernard plot’ (Bernard et al., 1976): the wetness gas ratio  $C_1/(C_2+C_3+C_4)$ , is reported as a function of the methane  $\delta^{13}C$ , together with a hypothetical two-endmembers mixing curve. Data reported here are the same as used in Ruffine et al., (2018b).

915  
 916  
 917  
 918  
 919  
 920  
 921  
 922  
 923  
 924  
 925  
 926  
 927  
 928  
 929  
 930  
 931  
 932  
 933  
 934  
 935  
 936  
 937  
 938  
 939  
 940  
 941  
 942  
 943  
 944  
 945  
 946



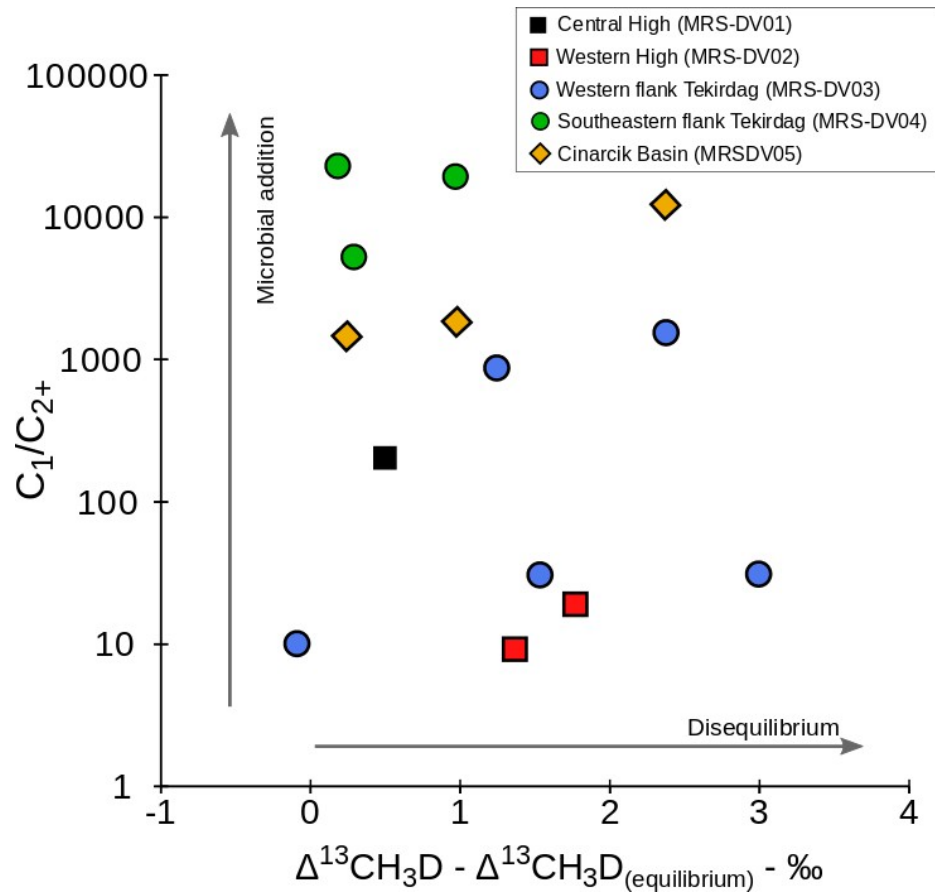
**Figure 3:** a) Methane bulk isotope composition.  $\delta^{13}C$  and  $\delta D$  measured on the Panorama are within uncertainty of these measurements. b) Methane isotopologue composition for SoM gas samples. The relationship between  $\Delta^{13}CH_3D$  and  $\Delta^{12}CH_2D_2$  and temperature is calculated following Young et al., (2016, 2017), see details in the Appendix. Despite the disagreement between the temperatures calculated for most samples, the distribution of  $\Delta^{12}CH_2D_2$ -based temperatures appear to be bi-modal, averaging at  $93 \pm 5^\circ C$  and  $152 \pm 22^\circ C$ , with few samples matching these temperatures for  $\Delta^{13}CH_3D$  as well. Note these two apparent temperatures roughly match the maximum temperatures reached by two of the main source rocks (i.e. organic-rich sediments) in the area, the Eocene Hamitabad Formation and the Oligocene Mezardere Formation (Huvaz et al., 2005; Gürgey, 2009).

947  
948  
949  
950  
951  
952  
953  
954  
955  
956  
957  
958  
959  
960  
961  
962  
963  
964  
965  
966  
967  
968  
969  
970  
971  
972  
973  
974  
975  
976  
977  
978

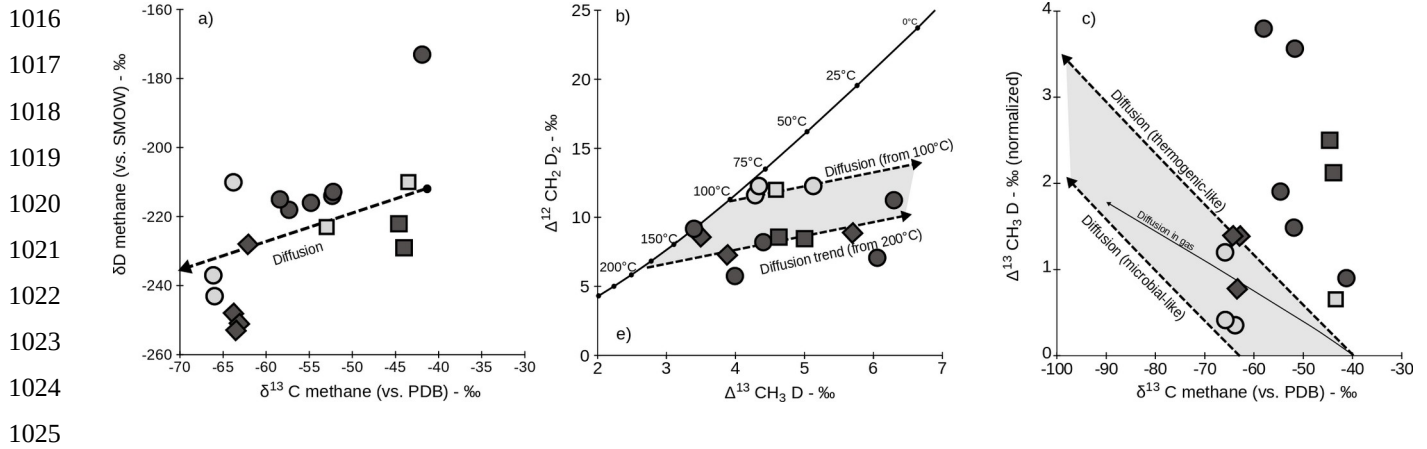


**Figure 4:** Methane isotopologue signatures produced by various strains of methanogens using different metabolic pathways (see details in Young et al., 2017; Giunta et al., 2019), shown with gases from the Sea of Marmara (this study) and with thermogenic-microbial gas mixtures from the Michigan Basin (Giunta et al., 2019). Culture of methanogens in laboratory have certainly not explored the whole variability of  $\Delta^{13}\text{CH}_3\text{D}$  and  $\Delta^{12}\text{CH}_2\text{D}_2$  values that can be obtained during microbial generation. Potential mixing curves are given as illustrations, assuming microbial end-members at the SoM are similar to those measured in laboratory. Note that mixing may result in non-linearity effects in the  $\Delta^{13}\text{CH}_3\text{D}$ - $\Delta^{12}\text{CH}_2\text{D}_2$  space (Young et al., 2016; Douglas et al., 2016), with a curvature depending on bulk isotopic compositions ( $\delta^{13}\text{C}$  and  $\delta\text{D}$ ) of end-members. With this simple exercise, it is shown that if attempting to fit SoM data with a mixing line having a microbial end-member similar to those measured in laboratory, then SoM gases would at most contain 60% microbial methane which seems inconsistent with extreme  $\text{C}_1/\text{C}_{2+}$  enrichment ( $>1000$ ). Instead, the data would suggest an in situ microbial end-member with a  $\Delta^{13}\text{CH}_3\text{D}$  of at least 6 ‰, in line with other observations of microbial methane in the deep biosphere (Wang et al., 2015; Inagaki et al., 2015; Ash et al., 2019).

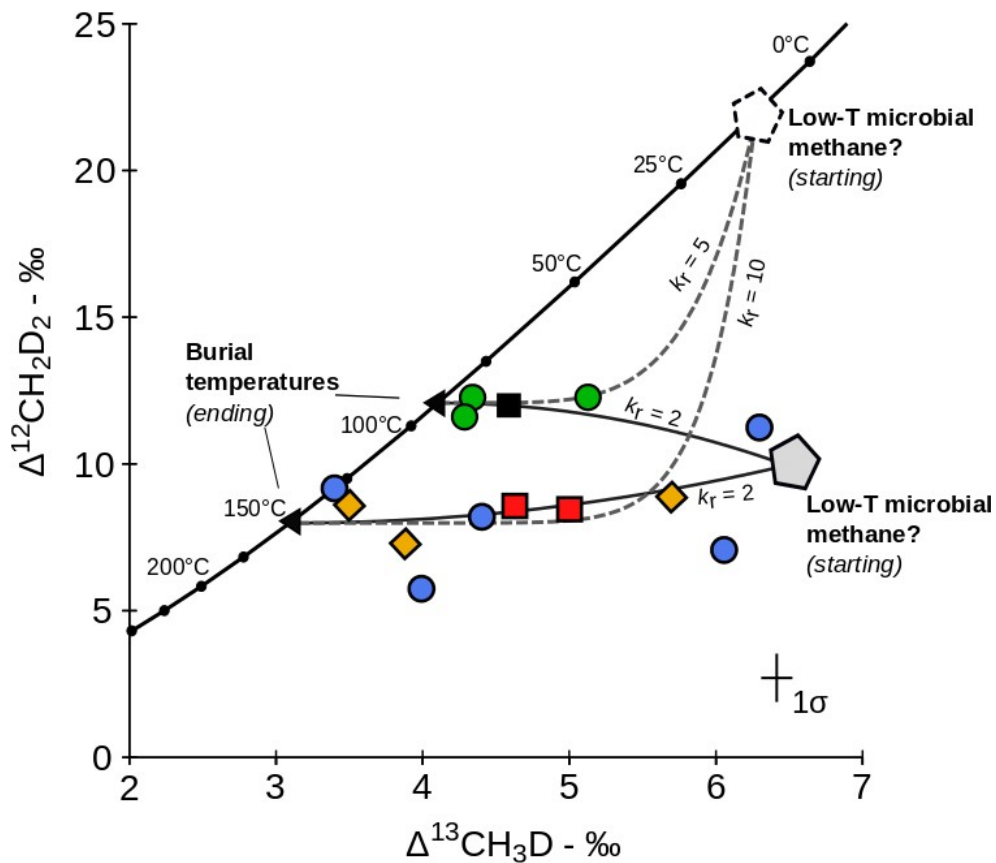
979  
980  
981  
982  
983  
984  
985  
986  
987  
988  
989  
990  
991  
992  
993  
994  
995  
996  
997  
998  
999  
1000  
1001  
1002  
1003  
1004  
1005  
1006  
1007  
1008  
1009  
1010  
1011  
1012  
1013  
1014  
1015



**Figure 5:** Wetness ratio ( $C_1/C_{2+}$ ) reported as a function of  $\Delta^{13}CH_3D - \Delta^{13}CH_3D_{(equilibrium)}$ .  $\Delta^{13}CH_3D_{(equilibrium)}$  is calculated such as it matches the equivalent temperature inferred from  $\Delta^{12}CH_2D_2$ . This is a convenient way to evaluate for each sample, the offset from the equilibrium in the  $\Delta^{13}CH_3D$ -axis, and to demonstrate that there are no apparent correlation with  $C_1/C_{2+}$ . Assuming that microbial methanogenesis should produce disequilibrium, as shown in all laboratory culture experiments (Wang et al., 2015; Stolper et al., 2015; Douglas et al., 2016; Young et al., 2017; Gruen et al., 2018; Giunta et al., 2019), then in case of mixing with a microbial source, one would expect positive relationship between the two parameters.



1026 **Figure 6:** Investigating the potential role of diffusion on SoM gases. Diffusion trends are plotted by  
 1027 solving the Fick's law in a semi-infinite space for each isotopologue. a) In a bulk  $\delta^{13}\text{C}$ - $\delta\text{D}$  space,  
 1028 diffusion should produce a 1:1 slope. b) In the  $\Delta^{13}\text{CH}_3\text{D}$  -  $\Delta^{13}\text{CH}_3\text{D}$  space, diffusion is also expected to  
 1029 produce a 1:1 slope. The SoM data may suggest two distinct diffusion slopes starting at two different  
 1030 equilibrium temperatures of 100 °C (gray symbols) and 200 °C (dark symbols). c)  $\Delta^{13}\text{CH}_3\text{D}$  as a  
 1031 function of bulk  $\delta^{13}\text{C}$ . Note that  $\Delta^{13}\text{CH}_3\text{D}$  data were normalized to their hypothetical starting  
 1032 equilibrium value, whether at 100 °C (grey symbols) or at 200 °C (dark symbols). The comparison of  
 1033 diffusive effects on singly and doubly-substituted methane isotopologues requires self consistency of  
 1034 diffusion coefficients assigned to each isotopologues. For singly-substituted methane isotopologues, we  
 1035 used  $\alpha_{17-16} = D(^{13}\text{CH}_4)/D(^{12}\text{CH}_4) = D(^{12}\text{CH}_3\text{D})/D(^{12}\text{CH}_4) = 0.997$ , as determined by [Prinzhofer and](#)  
 1036 [Pernaton, \(1997\)](#) for diffusion of methane in water. Following the framework of [Richter et al., \(2006\)](#),  
 1037 isotope fractionation factor associated to diffusion may be described as  $\alpha_{17-16} = (17/16)^\beta$ , where  $\beta$  an  
 1038 empirical parameter depending on the solvent in which diffusion takes place, would thus equals to  
 1039 0.05. Using this same  $\beta$  value for doubly-substituted isotopologues yields  $\alpha_{18-16} = D(^{13}\text{CH}_3\text{D})/D(^{12}\text{CH}_4)$   
 1040  $= D(^{12}\text{CH}_2\text{D}_2)/D(^{12}\text{CH}_4) = (18/16)^{-0.05} = 0.994$ . Though not considered likely in the context of the SoM,  
 1041 diffusion occurring in gas phase ( $\beta = 0.5$ ) would produce a different diffusion slope in the  $\Delta^{13}\text{CH}_3\text{D}$ -  
 1042  $\delta^{13}\text{C}$  space. In all cases, the variations observed in  $\Delta^{13}\text{CH}_3\text{D}$  should be associated with much larger  
 1043 variations in bulk  $\delta^{13}\text{C}$  than they actually are, precluding from considering diffusion as being a major  
 1044 process at play.



1070 **Figure 7:** Exploring the role of different relative rate of re-equilibration. Here we assume that spread  
 1071 to the right of the equilibrium curve reflect partial re-equilibration of  $\Delta^{12}\text{CH}_2\text{D}_2$  and  $\Delta^{13}\text{CH}_3\text{D}$  to burial  
 1072 temperatures of 90 °C and 150 °C. The relative rate is expressed as  $k_r = k_{12\text{CH}_2\text{D}_2}/k_{13\text{CH}_3\text{D}}$  (or =  $k_1/k_2$  in  
 1073 Equations 7 and 8). If assuming a starting isotopologue composition plotting on the equilibrium curve  
 1074 at an equivalent temperature of  $\sim 10$  °C (dashed-pentagon symbol), then  $k_r$  is required to be at least of  
 1075 5 to 10 to explain the data (gray dashed arrows). Alternatively, attempting to fit the data with  $k_r = 2$ , as  
 1076 suggested by *ab initio* calculations (see Appendices), implies that methane isotopologue signature prior  
 1077 to re-equilibration was plotting out of the equilibrium curve, perhaps with a  $\Delta^{12}\text{CH}_2\text{D}_2$  signature  
 1078 (coincidentally) not too different from equilibrium ‘ending’ signatures. For illustration, one possible  
 1079 out-of-equilibrium starting composition is reported here (grey-pentagon symbol) that would allow  
 1080 fitting the SoM data with  $k_r = 2$ .